

Central Lancashire Online Knowledge (CLoK)

Title	Permeability Jailbreak: A Deep Simulation Study of Hydraulic Fracture Cleanup in Heterogeneous Tight Gas Reservoirs
Type	Article
URL	https://clock.uclan.ac.uk/id/eprint/56015/
DOI	https://doi.org/10.3390/en18143618
Date	2025
Citation	Nasriani, Hamid Reza and Jamiolahmady, Mahmoud (2025) Permeability Jailbreak: A Deep Simulation Study of Hydraulic Fracture Cleanup in Heterogeneous Tight Gas Reservoirs. <i>Energies</i> , 18 (14). p. 3618.
Creators	Nasriani, Hamid Reza and Jamiolahmady, Mahmoud

It is advisable to refer to the publisher's version if you intend to cite from the work.
<https://doi.org/10.3390/en18143618>

For information about Research at UCLan please go to <http://www.uclan.ac.uk/research/>

All outputs in CLoK are protected by Intellectual Property Rights law, including Copyright law. Copyright, IPR and Moral Rights for the works on this site are retained by the individual authors and/or other copyright owners. Terms and conditions for use of this material are defined in the <http://clock.uclan.ac.uk/policies/>

Article

Permeability Jailbreak: A Deep Simulation Study of Hydraulic Fracture Cleanup in Heterogeneous Tight Gas Reservoirs

Hamid Reza Nasriani ^{1,*}  and Mahmoud Jamiolahmady ²¹ School of Engineering & Computing, University of Central Lancashire, Preston PR1 2HE, UK² Institute of Geoenergy Engineering, Heriot-Watt University, Edinburgh EH14 4AS, UK

* Correspondence: hrnasriani@uclan.ac.uk

Abstract

Ultra-tight gas reservoirs present severe flow constraints due to complex interactions between rock–fluid properties and hydraulic fracturing. This study investigates the impact of unconventional capillary pressure correlations and permeability jail effects on post-fracture cleanup in multiple-fractured horizontal wells (MFHWs) using high-resolution numerical simulations. A novel modelling approach is applied to represent both weak and strong permeability jail phenomena in heterogeneous rock systems. A comprehensive suite of parametric simulations evaluates gas production loss (GPL) and produced fracture fluid (PFF) across varying fracture fluid volumes, shut-in times, drawdown pressures, and matrix permeabilities. The analysis leverages statistically designed experiments and response surface models to isolate the influence of rock heterogeneity and saturation-dependent flow restrictions on cleanup efficiency. The results reveal that strong jail zones drastically hinder fracture fluid recovery, while weak jail configurations interact with heterogeneity to produce non-linear cleanup trends. Notably, reducing the pore size distribution index in Pc models improves predictive accuracy for ultra-tight conditions. These findings underscore the need to integrate unconventional Kr and Pc behaviour in hydraulic fracturing design to optimise flowback and long-term gas recovery. This work provides critical insights for improving reservoir performance and supports ambitions in energy resilience and net-zero transition strategies.



Academic Editor: Reza Rezaee

Received: 26 April 2025

Revised: 24 May 2025

Accepted: 18 June 2025

Published: 9 July 2025

Citation: Nasriani, H.R.; Jamiolahmady, M. Permeability Jailbreak: A Deep Simulation Study of Hydraulic Fracture Cleanup in Heterogeneous Tight Gas Reservoirs. *Energies* **2025**, *18*, 3618. <https://doi.org/10.3390/en18143618>

Copyright: © 2025 by the authors. Licensee MDPI, Basel, Switzerland. This article is an open access article distributed under the terms and conditions of the Creative Commons Attribution (CC BY) license (<https://creativecommons.org/licenses/by/4.0/>).

Keywords: permeability Jail; heterogeneity; flowback cleanup; hydraulic fracturing; fracturing fluid; capillary pressure; IFT; unconventional reservoirs

1. Introduction

Natural gas is widely recognised as a vital transitional energy source, playing a pivotal role in the global energy portfolio as economies navigate the complex path towards lower-carbon energy systems. Its prominence stems significantly from its combustion characteristics; among fossil fuels, it emits the least amount of carbon dioxide (CO₂) per unit of energy generated, approximately 50–60% less than coal and around 30% less than oil. This favourable emissions profile positions natural gas as an essential component in decarbonisation strategies, particularly for displacing higher-emitting coal in power generation and providing reliable, dispatchable power to complement the intermittency of renewable sources like solar and wind. Furthermore, it serves as a critical feedstock for various industrial processes and remains a primary fuel for residential and commercial heating in many regions.

However, the landscape of natural gas production has undergone a significant transformation. With the progressive maturation and depletion of conventional reservoirs—those characterised by relatively high permeability and porosity, allowing gas to flow more readily—the energy industry’s focus has necessarily shifted towards unlocking unconventional resources. These resources, particularly tight and ultra-tight gas formations, represent a substantial portion of the remaining global natural gas reserves. Tight gas reservoirs are typically defined by matrix permeabilities below 0.1 millidarcy (mD), while ultra-tight formations can exhibit permeabilities in the microdarcy or even nanodarcy (nD) range. Gas within these formations is trapped within complex, poorly connected pore networks, rendering natural flow rates commercially unviable without advanced stimulation techniques. Consequently, the economic development of these vast resources hinges critically on the successful application of technologies like horizontal drilling combined with multi-stage hydraulic fracturing, which create conductive pathways necessary to liberate the trapped gas and enable its flow to the wellbore. The inherent geological complexity and significant spatial variability (heterogeneity) within these formations further complicate appraisal and production optimisation efforts, directly impacting the effectiveness of stimulation and subsequent gas recovery [1]. Tight gas reservoirs (TGRs) represent a significant category of unconventional natural gas resources, characterised by natural gas trapped within reservoir rocks possessing exceptionally low matrix permeability. These formations, encountered globally, with major accumulations identified in North America (e.g., basins in the Rockies, Mid-Continent, Texas, and Appalachia), the Middle East (such as the Jafurah Basin in Saudi Arabia), China (including the Ordos and Tarim Basins), and parts of Europe, present extreme flow challenges that fundamentally distinguish them from conventional gas resources. The primary obstacle stems from their intrinsic petrophysical properties, notably matrix permeabilities typically falling within the microdarcy (10–3 Darcy) to nanodarcy (10–9 Darcy) range. This ultra-low permeability severely restricts the natural ability of gas to flow through the rock matrix towards a production well at economically viable rates.

Compounding this issue is the pronounced heterogeneity inherent in these reservoirs. This heterogeneity manifests across multiple scales, from macroscopic variations in depositional facies, diagenetic overprints, and the presence of natural fracture networks, to microscopic variations in mineralogy, grain size, and pore structure. Consequently, reservoir properties like porosity, permeability, capillary pressure, and mechanical characteristics can vary significantly both vertically and laterally, making reservoir characterisation, performance prediction, and stimulation design exceedingly complex.

Furthermore, the pore systems within tight formations often exhibit complex geometries. Unlike the relatively well-connected, larger pores typical of conventional reservoirs, TGRs frequently feature intricate networks of intergranular, intragranular, and dissolution pores, often interconnected by narrow, poorly sorted pore throats measuring in the micrometre to nanometre scale. Significant porosity may also be associated with clay minerals or organic matter (kerogen). This intricate pore architecture results in high tortuosity for flowing fluids and contributes to very high capillary pressures. These high capillary forces, combined with the small pore-throat sizes, are particularly detrimental during and after hydraulic fracturing operations. They can lead to the strong imbibition of aqueous fracturing fluids into the matrix adjacent to the created hydraulic fractures. This imbibition, coupled with potentially unfavourable relative permeability effects at high water saturation in the near-fracture region, can severely impede the flowback of the treatment fluid (fracture cleanup) and, more critically, hinder the subsequent flow of gas to the fracture. This phenomenon, where the effective permeability to gas near the fracture face is drastically reduced, sometimes approaching zero, due to trapped aqueous phases driven by capillary retention, is often referred to as ‘permeability jail’ or ‘water blocking’. It

represents a significant mechanism contributing to impaired well productivity, particularly in drier gas reservoirs where the initial water saturation is low, making the rock strongly water-wet and susceptible to imbibition [2–8].

Hydraulic fracturing has proven unequivocally essential for unlocking the economic production potential of natural gas stored within ultra-low-permeability tight gas formations. These reservoirs typically exhibit matrix permeabilities in the microdarcy to nanodarcy range, rendering them commercially non-viable without stimulation. The hydraulic fracturing process engineers high-conductivity conduits by injecting substantial volumes of fracturing fluid (FF)—predominantly water-based systems carrying proppant and chemical additives—at pressures exceeding the rock’s tensile strength and minimum in situ stress. This creates complex fracture networks that dramatically increase the contact area between the wellbore and the reservoir matrix, enabling hydrocarbon flow.

However, while the creation of these artificial fractures provides the necessary access to the matrix system, the subsequent recovery of the injected fracturing fluid, a critical phase termed flowback or cleanup, is frequently and significantly inefficient, particularly in tight gas settings. Industry data and numerous studies report that often, only a small percentage (sometimes less than 30–50% and occasionally much lower) of the injected fluid volume is recovered during the operational lifetime of the well. This inefficiency is not merely an operational curiosity but a major technical challenge rooted in complex multiphase flow dynamics and fluid–rock interactions within the confined pore spaces and the newly created fracture system.

Low cleanup efficiency inevitably leads to substantial residual water retention within both the propped fracture network and, critically, the adjacent reservoir matrix invaded by fluid leakoff. This retained water saturation (S_w) near the fracture face occupies pore space and alters the multiphase flow characteristics dramatically. According to fundamental principles of relative permeability, an increase in water saturation directly leads to a decrease in the relative permeability to gas (k_{rg}). This impairment restricts the ability of gas molecules to desorb (if applicable), diffuse through the matrix pore network, and enter the fracture system for transport to the wellbore. This phenomenon is often described as a ‘water block’.

In particularly challenging scenarios, characterised by very low matrix permeability, strong capillary forces inherent in small pore throats, potentially altered wettability due to FF additives, and high shut-in times allowing deep invasion, the reduction in gas relative permeability can become extreme. This severe impairment is sometimes referred to as the ‘permeability jail’ effect, where the near-fracture zone becomes so water-saturated that gas mobility is drastically reduced, effectively trapping significant gas volumes deeper within the matrix behind a barrier of high water saturation. Consequently, this leads to significant gas production loss (GPL), manifesting as lower initial production rates, steeper decline curves, and a reduced estimated ultimate recovery (EUR) compared to scenarios with efficient cleanup.

The severity of cleanup inefficiency and the associated GPL is exacerbated under certain conditions. Low drawdown operations—where the pressure differential between the reservoir and the wellbore is minimal—provide insufficient viscous forces to effectively overcome the capillary forces holding the water phase within the tight pore structure. Cleanup is also inherently more challenging in formations with intrinsically poor fluid mobility (low k/μ , where k is permeability and μ is viscosity) and strong capillary characteristics, which are defining features of tight gas reservoirs. Furthermore, reservoir heterogeneity, encompassing spatial variations in petrophysical properties like permeability, porosity, and capillary pressure, complicates fluid leakoff patterns and subsequent flowback, leading to uneven cleanup and localised regions of severe water trapping. Chem-

ical interactions between the fracturing fluid components and the formation minerals (e.g., clay swelling, fines migration, precipitation of scales) can also contribute to formation damage, further impeding both fluid recovery and hydrocarbon production [9–16].

1.1. The Permeability Jail Phenomenon

One of the most significant findings emerging from investigations into fluid flow within ultra-tight formations, particularly relevant during the critical phase of hydraulic fracture cleanup, is the identification and characterisation of the ‘permeability jail’. This concept is central to understanding multiphase flow dynamics in reservoirs characterised by nano- to microdarcy matrix permeability. It refers to a specific, often intermediate, range of fluid saturations within the complex pore network where the relative permeabilities of both the aqueous phase (typically invaded water-based fracturing fluid) and the hydrocarbon gas phase become simultaneously and exceptionally low, frequently approaching negligible values relative to their single-phase permeabilities. In Figure 1, the conceptual differences between the relative permeability and capillary pressure functions for conventional formations and those for unconventional (tight and ultra-tight) reservoirs are illustrated.

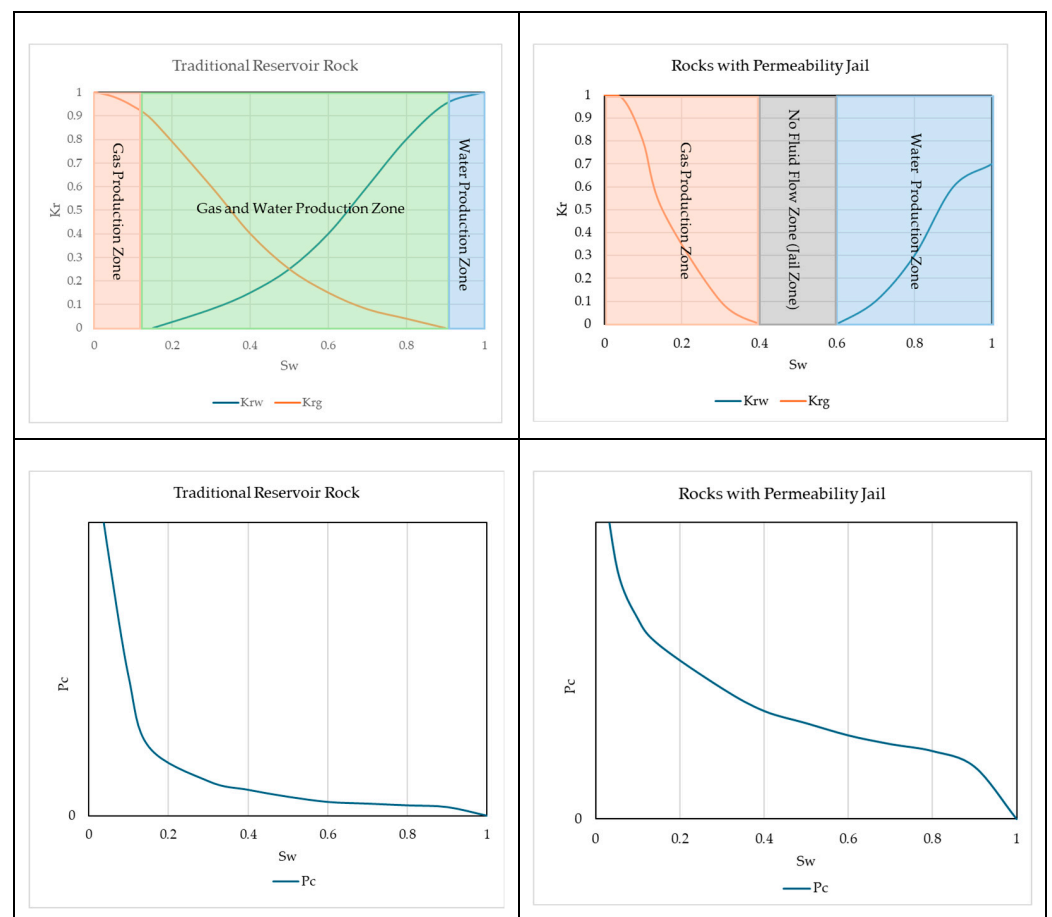


Figure 1. Capillary pressure and relative permeability curves in traditional and unconventional reservoir rocks.

In conventional reservoirs, the critical water saturation (S_{wc}) and irreducible water saturation (S_{wirr}) typically exhibit minimal disparity, often allowing the two terms to be used interchangeably. However, in tight and ultra-tight formations, a pronounced divergence between these two saturations is commonly observed, with the critical water saturation

being substantially higher than the irreducible water saturation. A clear understanding of these concepts is fundamental for accurately describing multiphase flow behaviour:

- **Critical Saturation:** The critical saturation—whether for water (S_{wc}), gas (S_{gc}), or oil (S_{oc})—defines the minimum saturation level at which a phase becomes mobile under increasing saturation conditions. This property is inherently associated with relative permeability curves and directly influences the onset of fluid flow through the porous medium.
- **Irreducible Saturation:** The irreducible saturation pertains to the lowest saturation value at which a phase remains after extensive displacement by another phase, typically determined through capillary pressure measurements at high pressures during special core analysis. It is a fundamental characteristic of capillary pressure curves. Irreducible saturations include irreducible water saturation (S_{wirr}), residual oil saturation (S_{or}), trapped gas saturation (S_{gr}), and trapped oil saturation (also denoted as S_{or}). The connate water saturation—representing the naturally occurring water saturation in situ—is often approximated to S_{wirr} .

According to standard industry definitions, such as those outlined in the SPE Petroleum Resources Management System (PRMS) and SPE E&P Glossary, the irreducible saturation (S_{wirr}) refers to the lowest water saturation at which water becomes immobile under increasing gas or oil saturation, often associated with the capillary pressure drainage curve. In contrast, the critical water saturation (S_{wc}) marks the onset of water beginning to flow during increasing saturation (imbibition process), as reflected in relative permeability curves. The disparity between these saturations is particularly prominent in ultra-tight formations due to high capillary forces and pore confinement effects. This distinction is essential for characterising the ‘permeability jail’ window where both gas and water mobilities are significantly hindered. For further clarity and adherence to industry norms, these terms are used as defined in the SPE Glossary of Terms [17].

In tight and ultra-tight reservoirs, the considerable difference between critical and irreducible saturations is a manifestation of the unique pore structure, which is characterised by exceedingly low permeability and highly tortuous pore networks. This restricted pore geometry leads to significant interaction and interference between fluid phases, especially within the constricted pore throats. As a result, critical gas saturation also increases notably.

Consequently, there exists a saturation interval where both gas and water phases exhibit severely reduced or minimal relative permeabilities. This phenomenon creates a flow-restrictive environment known as the permeability jail. Within this saturation window, fluid mobility is drastically impaired, posing significant challenges to hydrocarbon production and fracturing fluid cleanup in unconventional reservoirs.

This dramatic reduction in the ability of either phase to flow is a direct consequence of heightened capillary forces and complex phase interference effects prevalent in the tight pore structures. High capillary pressures, dictated by the small pore-throat sizes and fluid–rock interactions (wettability), effectively trap the wetting phase (often water or frac fluid filtrate) within the smaller pores and pore throats. Concurrently, this trapped, immobile water phase significantly increases the tortuosity of the pathways available for the non-wetting gas phase and occupies pore volume, drastically reducing the effective permeability available for gas flow. The result is a state of phase trapping, where substantial volumes of both fracturing fluid and potentially valuable formation gas become effectively immobilised within the reservoir matrix surrounding the hydraulic fractures, as well as potentially within the proppant pack itself under certain conditions.

The practical implication of entering this permeability jail saturation window during flowback is severely impaired multiphase flow towards the wellbore. This phenomenon acts as a major bottleneck for efficient fracture cleanup, directly contributing to several

detrimental outcomes: notably high volumes of retained fracturing fluid ('load recovery' issues), significantly prolonged cleanup durations extending for weeks or months, a reduction in the effective flowing length and conductivity of the created hydraulic fractures, and, consequently, diminished initial gas production rates and potentially lower estimated ultimate recovery (EUR) for the well. Understanding the precise saturation ranges, the governing mechanisms (influenced by factors such as rock wettability, interfacial tension, pore size distribution, fluid viscosity ratios, applied drawdown pressure, and temperature), and the impact of reservoir heterogeneity on the severity of the permeability jail is therefore paramount. Advanced numerical simulation studies, often incorporating sophisticated relative permeability and capillary pressure models derived from experimental core analysis or pore-network modelling, are essential tools for quantifying the impact of the permeability jail under diverse reservoir conditions and for evaluating the efficacy of potential mitigation strategies, such as the use of surfactants, mutual solvents, or optimised flowback procedures, aimed at minimising phase trapping and accelerating the recovery of hydrocarbons from these challenging unconventional resource plays [18–25]. Shanley et al. (2004) documented that in many tight gas formations, critical water saturation (S_{wc}) and irreducible water saturation (S_{wirr}) are no longer equivalent, as they often are in conventional reservoirs, but diverge considerably, creating a no-flow saturation zone [26–30].

Cluff and Byrnes (2010) further described how this phenomenon emerges from complex pore-throat geometry, high capillary pressure, and hysteresis effects, which together suppress both water and gas mobility [6]. Gdanski and Walters (2010) demonstrated in simulations that this immobility zone can be persistent even under high drawdown, particularly when phase trapping and wettability hysteresis are active [10,31]. Gong et al. (2022) and Lai et al. (2023) provided experimental and numerical evidence that rocks with lower permeability tend to exhibit broader and more severe jail regions [32,33].

This immobility zone introduces fundamental challenges to cleanup operations. Field observations, such as those by Assiri and Miskimins (2014), revealed that desiccated formations—those with $S_w < S_{wirr}$ —can exhibit substantial productivity impairment following hydraulic fracturing, with gas rates reduced by up to 44% [34]. The permeability jail, therefore, must be treated as a key factor in the simulation, modelling, and operational design of stimulation treatments [11–13,35].

1.2. Advances in Capillary Pressure and Relative Permeability Models

Conventional capillary pressure (P_c) and relative permeability (K_r) models, which were primarily developed and validated using data from moderately permeable formations like conventional sandstones, are often demonstrably insufficient for accurately representing fluid behaviour within ultra-tight systems such as shales and tight gas sands. These traditional models arose from experimental observations in media where pore sizes are typically in the micron range and pore networks, while complex, often exhibit a degree of homogeneity and connectivity that allows for simplified macroscopic representation. Consequently, their application to ultra-tight systems—characterised by pervasive nanoscale pore throats (often below 100 nm), intricate and poorly connected pore networks, significant multiscale heterogeneity, and high surface-area-to-volume ratios leading to dominant fluid–rock interactions—proves fundamentally inadequate for capturing the governing physics.

Classical formulations, such as the widely adopted van Genuchten or Brooks–Corey models, are mathematically predicated on assumptions that yield relatively smooth, monotonic P_c –saturation (S_w) and K_r – S_w relationships. They typically presuppose limited hysteresis between drainage (fluid displacing wetting phase) and imbibition (wetting phase displacing fluid) cycles and often neglect or oversimplify the profound impact of pore wall proximity, known as confinement effects, on fluid properties (like interfacial tension

and viscosity) and phase behaviour, which become critically important at the nanoscale. Furthermore, the strong fluid–solid interactions, influenced by mineralogy (e.g., clays) and organic matter content, can lead to complex wettability states (mixed or fractional wettability) that are poorly represented by the simple contact angle assumptions implicit in these older models [35–37].

This inherent simplification means that they fundamentally fail to capture the strong non-linearity frequently observed in experimental Pc and Kr data derived from tight rock samples. This non-linearity is not mere measurement noise but reflects complex pore-level displacement mechanisms, including abrupt piston-like displacements in nanopores, cooperative pore filling/emptying events, and significant phase trapping (snap-off) influenced by high pore-body-to-throat aspect ratios and tortuous, poorly connected pathways. Furthermore, these conventional models struggle to represent the severe, saturation-dependent flow inhibition that characterises tight rocks, particularly at high wetting-phase saturations. In these systems, capillary forces, magnified within the nanopores, often dominate over the viscous forces driving flow, leading to very high irreducible water saturations and significant multiphase flow interference that drastically reduces the mobility of the non-wetting phase (gas or oil). This specific limitation is particularly critical when analysing processes like hydraulic fracture cleanup, where the retention of aqueous fracturing fluids due to extremely high capillary entry pressures significantly impedes the flowback process and severely reduces the effective permeability to hydrocarbons near the fracture face—a primary mechanism contributing to the detrimental ‘permeability jail’ effect, ultimately hindering well productivity [36–42].

Recent work has advanced the development of unconventional Pc and Kr models that integrate these anomalies [43–47]. For example, He et al. (2025) and Sharifigaliuk et al. (2023) have presented modified capillary pressure curves that account for pore-throat connectivity and non-wetting-phase invasion resistance [48,49]. Their work, coupled with high-resolution micromodel visualisation studies [50,51], has helped define the true shape of Pc curves under drainage and imbibition in tight sandstones.

Nasriani et al. explored the implementation of weak and strong permeability jail scenarios in numerical simulators using modified Corey-type Kr curves with crossover regions suppressed. Their work aligns with findings by Shaoul et al. (2011), who modelled jail zones with a 20–30% saturation window of near-zero mobility [11–14,35,52–62]. Lai et al. (2023) further proposed a generalised method to extract jail parameters from laboratory Kr measurements and integrate them into compositional reservoir simulators [32,63].

While direct experimental validation of the permeability jail concept is still evolving, our implementation of modified Corey-type relative permeability curves is informed by existing core-scale studies on tight sandstones and shales. In particular, works by several research teams [6,32,33] provide Kr/Pc measurements that reveal a saturation interval with near-zero mobility consistent with the simulated jail zones. These studies observe a significant divergence between Swirr and Swc and support the modelling assumption of mobility suppression within a defined saturation window. Our parametric model captures this behaviour in a controlled framework, though future work integrating direct laboratory Kr-Pc measurements from core plugs would strengthen model realism.

These models have profound implications. Where traditional models overestimate flowback, the use of permeability jail-aware models reveals that even high-pressure drawdown may fail to displace FF effectively unless auxiliary forces (e.g., osmotic gradients, chemical alteration, or surfactants) are employed. This understanding has shifted engineering focus towards mitigating jail effects via fluid design, optimal drawdown strategy, and extended soaking periods.

1.3. Operational Levers: Drawdown Pressure and Shut-In Time

Drawdown pressure and shut-in time are key operational variables that influence fracture fluid recovery. Holditch (1979) first showed that inadequate drawdown relative to P_c can result in total gas blockage by trapped FF [9]. May et al. (1997) later demonstrated that fracture conductivity is more impactful than the pressure gradient in many cases [64]. This is supported by Lolon et al. (2003), who found that the effective fracture length—controlled by F_{cd} —is the dominant factor governing cleanup [65].

Recent investigations have focused on the impact of soaking time. Jiang et al. (2024) and Li et al. (2023) showed that controlled shut-in enhances capillary-driven imbibition, improving long-term gas production even at the cost of higher water retention [66–68]. This is particularly beneficial in formations with moderate-to-weak jail effects, where some matrix flow is possible. Ghanbari and Dehghanpour (2016) and Jing et al. (2022) also observed that early high flowback rates often correlate with reduced gas recovery, as rapid flowback may prevent deeper imbibition and fracture unblocking [69–71].

Thus, many operators now employ adaptive flowback protocols—low initial drawdown followed by gradual ramp-up. These strategies are increasingly integrated with real-time surveillance tools and predictive simulators to maximise cleanup efficiency while preserving fracture integrity [13].

We acknowledge that the Brooks–Corey model, although widely used and computationally efficient, may not fully capture confinement effects and wettability hysteresis that become prominent in nanoporous media. Recent advances employing pore-network models and molecular dynamics simulations have demonstrated that in nanodarcy systems, fluid behaviour departs significantly from classical assumptions due to surface force dominance, non-continuum effects, and contact angle variability. Alternative formulations such as the van Genuchten–Mualem model, especially when adapted for mixed-wet or low-permeability systems, offer enhanced fidelity in such regimes. Nonetheless, the Brooks–Corey framework was selected in this study to enable systematic parametric control and facilitate direct comparison with prior core-derived and field-applied datasets. Future work may incorporate dual-scale models or pore-level upscaling techniques to reflect the full complexity of gas–liquid transport in nano-confined systems.

1.4. Transition from Single to Multiple-Fractured Horizontal Wells (MFHWs)

Historically, most cleanup studies examined single-fracture or single-vertical-well configurations. However, with the widespread adoption of long horizontal wells with multiple fractures, cleanup behaviour has become more complex. Each fracture may interact with others, compete for drawdown, and exhibit varying cleanup dynamics depending on local matrix properties.

Analytical models [72], salt concentration tracers [73], and flowback characterisation methods [74] have all contributed to a better understanding of MFHW systems. These studies revealed that non-uniform cleanup among fractures is common, and fracture interference or heel-biased fluid intake can lead to suboptimal performance.

In response, recent simulation studies have expanded into full-field MFHW configurations, integrating variable fracture spacing, matrix heterogeneity, and permeability jail effects. These models highlight the need for tailored stimulation and flowback strategies that optimise across the entire well length, rather than treating fractures independently [12,14,35,75].

1.5. Novel Contributions and Research Gaps Addressed

Several research gaps remained unaddressed prior to this study. Most earlier models did not account for the full spectrum of ultra-tight matrix behaviour under coupled P_c – K_r

dynamics. Capillary pressure correlations were often applied outside of valid parameter ranges, and Kr curves were either too simplified or lacked hysteresis representation.

This research integrates weak and strong jail behaviours into a statistically robust simulation framework, incorporating Latin Hypercube Sampling and over 384,000 simulations. It evaluates 12 parameters, including Pc shape, relative permeability crossover, fracture conductivity, matrix heterogeneity, shut-in time, and fluid volume. The resultant response surface models offer engineers predictive tools for gas production loss (GPL) and fracture fluid recovery (PFF) under realistic MFHW configurations [12,14,35].

By incorporating recent Pc/Kr model developments and validating them under multi-variable interaction, this study offers both academic novelty and direct industrial relevance. It aligns with REF2029 expectations for originality, significance, and impact, and contributes directly to reservoir simulation practices, hydraulic fracture optimisation, and post-fracture management in ultra-tight gas systems. Building upon the understanding of multiphase flow complexities during hydraulic fracture cleanup, the work by Nasriani et al. provides a significant contribution to modelling efforts in heterogeneous tight gas reservoirs. They specifically addressed the challenging phenomenon known as ‘permeability jail’, which is particularly detrimental to the efficient recovery of hydrocarbons following stimulation treatments. Permeability jail arises from high capillary pressures within the tight pore matrix, leading to the trapping of aqueous fracturing fluids near the newly created fracture faces. This trapped water saturation drastically reduces the relative permeability to gas, effectively creating a barrier—the ‘jail’—that hinders gas flow towards the fracture and ultimately to the wellbore, thereby delaying production and potentially damaging long-term recovery.

Nasriani et al. explored how to quantitatively represent this critical effect within numerical reservoir simulators. Their methodology focused on the careful manipulation of relative permeability (Kr) curves, which govern the simultaneous flow of different fluid phases. Recognising that standard models like the Corey correlation might not adequately capture the severe phase interference effects observed in ultra-low-permeability systems, they implemented modified Corey-type Kr curves. A key aspect of their modification involved the suppression of the crossover region typically present in standard Kr curves. Suppressing this region, where both phases theoretically exhibit non-zero mobile saturations simultaneously, allows for a more pronounced representation of phase trapping, mimicking conditions where one phase (in this case, the injected water) can significantly impede or almost entirely block the flow of the other phase (gas) at relatively low saturations of the blocking phase.

Furthermore, they differentiated between ‘weak’ and ‘strong’ permeability jail scenarios by adjusting the parameters within these modified Kr functions [13]. This allowed them to simulate varying degrees of water trapping intensity, reflecting potential variations in rock properties, wettability, and fluid interactions across different reservoir zones or under different operational conditions. By incorporating these distinct, physically motivated Kr curve representations into their simulation framework, their study offered a valuable tool for investigating the sensitivity of fracture cleanup efficiency and subsequent gas production profiles to the severity of the permeability jail effect within complex, heterogeneous tight gas reservoir models. This approach enables a more realistic assessment of post-fracturing well performance and aids in optimising fracturing fluid selection and flowback strategies to mitigate the adverse impacts of water blockage.

2. Materials and Methods

To help us walk through the research approach and make the terminology clear, a flowchart (Figure 2) has been put together. Essentially, the first step was really digging

into the tricky aspects of how fluids move in these tight and ultra-tight rocks, specifically getting a handle on unconventional relative permeability (K_r) and capillary pressure (P_c) behaviours and also accounting for how much rock properties can vary from place to place (heterogeneity).

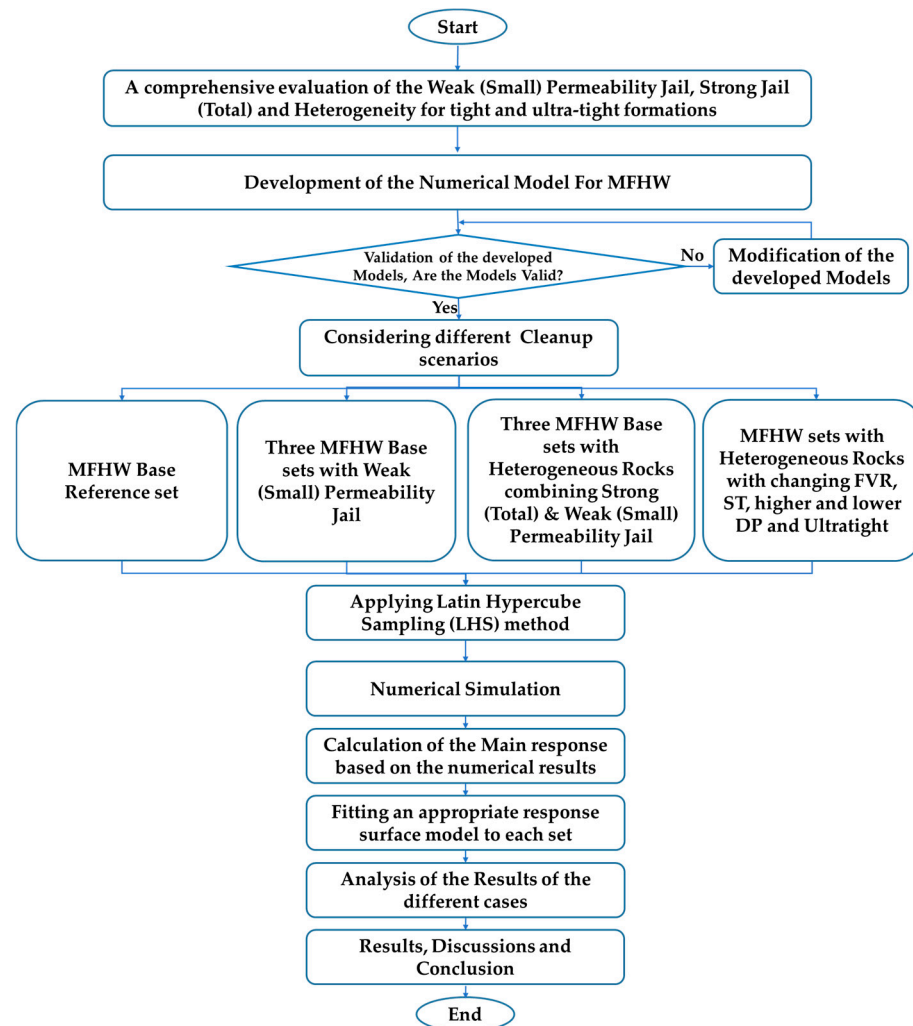


Figure 2. The workflow of the study.

With this groundwork laid, a specialised computer model representing a horizontal well with multiple hydraulic fractures was developed and used. We adapted and refined a setup initially developed in our previous research work [11,13]. The basic size and layout of this model are detailed in Table 1, and we have confirmed that it gives reliable results through validation steps described in separate work.

Table 1. MFHW model.

Lf (m)	Wf (m)	Horizontal Length (m)	Number of Fractures	Xres (m)	Yres (m)	Zres (m)
90	0.004	600	7	2000	2000	40

Once we were confident in the model, we set up a series of twelve distinct simulation runs, or scenarios, designed to explore different facets of fracture cleanup and the ‘permeability jail’ phenomenon. These scenarios were carefully chosen:

- **Scenario 1:** Started with a baseline case using typical unconventional capillary pressure data.

- **Scenarios 2–4:** Looked at situations representing a ‘weak’ permeability jail effect, systematically varying a key two-phase flow parameter (related to residual fluid or flow impairment, specified as 30%, 20%, and 10% values) to see how it influenced outcomes.
- **Scenarios 5–7:** Introduced geological realism by simulating three different types of heterogeneous rock formations, each containing a mix of areas prone to strong and weak permeability jail effects.
- **Scenarios 8–12:** Took one of the heterogeneous rock types (Rock 2) and pushed it further, exploring the sensitivity to operational factors and reservoir quality. We tested the impact of using a larger fracture volume (higher FVR, Scenario 8), letting the fluid soak for longer before flowback (extended soaking time, Scenario 9), changing the production pressure drawdown (lower pressure drawdown, Scenario 10; higher pressure drawdown, Scenario 11), and, finally, simulating an even tighter formation (ultra-tight formation, Scenario 12).

Within the scope of this investigation into multiphase flow behaviours, it is important to underscore the computational foundation laid for each scenario explored. A substantial collection, specifically one thousand individual simulation runs, was executed for every defined set or case being studied.

In carrying out these simulations, careful attention was given to exploring the parameter space adequately. Twelve key variables, identified as having a significant influence on the system’s behaviour (parameters like fracture conductivity, matrix permeability, capillary entry pressure characteristics, or relative permeability curve shapes), were systematically adjusted across their plausible operational- or reservoir-condition ranges. The precise boundaries defining the variation for each of these influential factors are meticulously documented for reference in Table 2. The fracture conductivity range ($K_f = 1\text{--}30$ Darcy) used in the simulation study reflects values reported by several international service companies actively engaged in hydraulic fracturing operations across North America and the Middle East. These values were derived from laboratory measurements and field-calibrated models, including proppant pack conductivity tests under representative closure stresses. Although the upper bound may exceed typical averages, it is intended to account for high-conductivity fracture segments, especially near the wellbore or in fractures stimulated using advanced proppant transport techniques. This range ensures model generality across a wide spectrum of reservoir and operational conditions.

Table 2. The parameters’ variation ranges.

Parameter	Min	Max
k_f (D)	1	30
k_m	1 μ D	100 μ D
λ	1	4
IFT (mNm/m)	2	50
n_{gm}	1.5	5
n_{wm}	1.2	4
k_{maxg}	0.5	1.0
k_{maxw}	0.05	0.6
n_{gf}	1.5	5
n_{wf}	1.2	4
k_{maxg}	0.5	1.0
k_{maxw}	0.1	0.75

For those seeking a deeper dive into the statistical underpinnings of how these parameter combinations were selected, a comprehensive treatment of the sampling method-

ologies employed is provided in the cited work [11,13]. It can be confirmed that the Latin Hypercube Sampling (LHS) technique—a method well-suited for efficiently exploring multi-dimensional parameter spaces—was utilised across all scenarios to generate the specific input values for the multitude of simulation runs.

Following the completion of this extensive simulation campaign, the resulting data from each set did not stand alone. Instead, a mathematical surface methodology, akin to response surface modelling, was applied. The objective here was the development and calibration of an accurate mathematical model capable of representing the complex relationships observed between the input parameters and the simulation outputs for each set.

Ultimately, the insights and findings derived from these carefully constructed simulation sets were subjected to thorough examination and interpretation. To maintain clarity regarding the specific conditions and configurations investigated, a detailed list itemising the analysed sets is provided in Table 3.

Table 3. Unconventional sets.

Set Name	No. of Fractures	Horizontal Length (m)	DP (Psi)	FVR	Shut-In Time (days)	Kf (D)	Km (μ D)	Lambda
Default Values	3	600	1000	2	2	1–30	1–100	1–4
Set 30	7	✓	✓	✓	✓	✓	✓	0.3–1.5
Set 34 weak jail, two phase 30%	7	✓	✓	✓	✓	✓	✓	0.3–1.5
Set 35 weak jail, two phase 20%	7	✓	✓	✓	✓	✓	✓	0.3–1.5
Set 36 weak jail, two phase 10%	7	✓	✓	✓	✓	✓	✓	0.3–1.5
Set 37 mixed 1	7	✓	✓	✓	✓	✓	✓	0.3–1.5
Set 38 mixed 2	7	✓	✓	✓	✓	✓	✓	0.3–1.5
Set 39 mixed 3	7	✓	✓	✓	✓	✓	✓	0.3–1.5
Set 40 mixed 2	7	✓	✓	10	✓	✓	✓	0.3–1.5
Set 41 mixed 2	7	✓	✓	✓	20	✓	✓	0.3–1.5
Set 42 mixed 2	7	✓	100	✓	✓	✓	✓	0.3–1.5
Set 43 mixed 2	7	✓	4000	✓	✓	✓	✓	0.3–1.5
Set 44 mixed 2	7	✓	✓	✓	✓	✓	0.1–10	0.3–1.5

2.1. Model Development and Validation

To investigate the intricate process of fluid cleanup in horizontal wells stimulated with multiple hydraulic fractures (MFHW), a numerical simulation model was carefully constructed using the ECLIPSE 100 reservoir simulator [76]. The foundational mathematical equations and the underlying physical principles integrated within the ECLIPSE framework, which govern fluid flow in porous media, are extensively documented in existing research [76] and form the basis of this modelling effort.

In this study, the fractured well is represented as a multiple-fractured horizontal well (MFHW) configuration, comprising seven uniformly spaced, planar bi-wing fractures along a 600-m horizontal lateral. Each fracture extends 90 m on either side of the wellbore, with a constant aperture of 0.004 m. This idealised fracture geometry is illustrated schematically in Figure 3.

Within this newly developed simulation framework, representing a pre-fractured state, a 600 m horizontal wellbore was defined, intersected by seven distinct hydraulic fractures. A significant decision in the model construction was the use of local grid refinement (LGR) techniques specifically concentrated around these fracture zones. This

approach was favoured over a more computationally intensive global grid refinement strategy. The selection of LGR was driven by the need to accurately capture the highly localised and complex flow behaviour changes within the stimulated reservoir volume (SRV)—the area immediately surrounding the fractures—while maintaining manageable simulation run times.

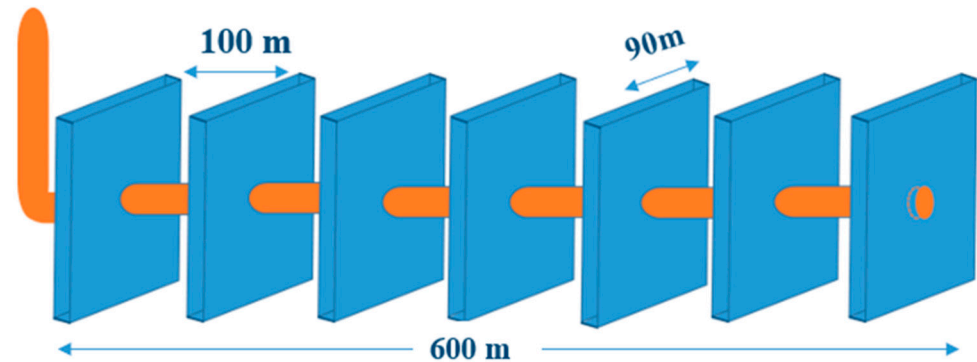


Figure 3. The modelled MFHW.

The reservoir system was initialised with a pressure condition of 7500 psi. The rock matrix itself was characterised by an average porosity of 15%. Specific details regarding the dimensions and geometric configuration of the numerical model components are systematically laid out in Table 1, while a visual schematic of the overall model setup is provided in Figure 3. It should be noted that the simulation ‘set numbers’ mentioned simply reflect the chronological order in which these specific simulations were executed as part of a larger, more comprehensive investigative study, elements of which extend beyond the scope of this particular discussion.

Focusing on the post-fracturing phase simulation, the model was designed to mimic the flowback period. During this stage, the production of both the native reservoir gas and the injected fracturing fluid (identified as water in this case) was simulated by applying a controlled flowing pressure condition at the wellbore’s bottom hole. As detailed in Table 1 and visualised in Figure 3, each induced fracture was assigned a half-length of 90 m, extending outwards from the wellbore into the formation.

For the fracturing fluid (water), key fluid properties were defined: a compressibility value of $5.0 \times 10^{-6} \text{ psia}^{-1}$ was utilised, alongside a viscosity of 0.5 centipoise (cp). In the established base reference case simulations for this MFHW scenario, the total volume of fracturing fluid injected during the simulated fracturing stage was deliberately set to be twice the calculated geometric volume of the created fractures. A crucial operational sequence incorporated into the simulation workflow was a mandatory two-day well shut-in period. This period was imposed immediately following the completion of fracturing fluid injection and, crucially, before the commencement of the flowback and production phase.

The methodology for validating the foundational amended VW model and its associated governing equations, upon which this MFHW study builds, has been thoroughly addressed in prior work [12]. To specifically establish confidence in the current MFHW simulation model, its predictive accuracy was assessed. This was achieved by comparing the simulated wellbore pressure behaviour over production time against the results obtained from a recognised analytical model designed for MFHW performance prediction [11].

The predicted bottom-hole flowing pressure (P_{wf}) from the numerical simulation against the analytical model’s prediction as a function of production time is represented elsewhere [11,12,14]. The remarkably close alignment, evidenced by the overlapping nature of the two curves, serves as strong support for the numerical simulation model’s validity and accuracy in representing the system’s behaviour.

It is pertinent to emphasise that this comprehensive study delves into the influence of twelve distinct parameters recognised for their significant impact on post-fracturing cleanup processes. Among these twelve, the first eight parameters directly pertain to the characterisation of two-phase relative permeability (K_r) using the well-established Brooks–Corey relationship. These include the critical endpoint saturations and the characteristic exponents for both the gas and water phases.

Furthermore, the capillary pressure (P_c) characteristics within the rock matrix are governed by three additional parameters under investigation: the intrinsic permeability of the matrix (K_m), the interfacial tension (IFT) between the gas and water phases, and the pore size distribution index (λ), which reflects the heterogeneity of the pore network. The final parameter considered in this sensitivity analysis is the permeability assigned to the hydraulic fractures themselves (K_f). The specific ranges over which these twelve parameters were varied during the simulation studies are systematically catalogued in Table 2. However, it is important to clarify that within any single set of simulation runs, six specific parameters—namely, the differential pressure (DP), the matrix porosity, and the critical water (S_{wc}) and gas (S_{gc}) saturations within both the matrix and the fracture domains—were held constant.

The mathematical formulations defining the capillary pressure and the related threshold (or entry) pressure used within the model are represented by Equations (1) and (2), respectively, drawing upon established theoretical frameworks [42,77]. Concurrently, the relationships describing the relative permeability of gas and water as functions of saturation are based on the seminal work by Brooks and Corey’s team, expressed mathematically in Equations (3) and (4). To systematically explore the parameter space defined in Table 2, input datasets for the simulations were generated using either Factorial Fractional Sampling (FFS) or Latin Hypercube Sampling (LHS) techniques, ensuring a robust investigation of parameter sensitivities [41,42,77].

$$\frac{P_d}{IFT} = 0.0075 \times K^{-0.5} \quad (1)$$

- Interfacial tension (IFT)
- K_m measured in mD

$$\left(\frac{P_d}{P_c}\right)^\lambda = \frac{S_w - S_{wr}}{1 - S_{wr}} \quad (2)$$

$$k_{rw} = K_{maxw} \times \left(\frac{S_w - S_{wr}}{1 - S_{wr} - S_{gr}}\right)^{nw} \quad (3)$$

$$k_{rg} = K_{maxg} \times \left(\frac{S_g - S_{gr}}{1 - S_{wr} - S_{gr}}\right)^{ng} \quad (4)$$

To thoroughly investigate the influence exerted by pressure drop (DP) on the efficiency of the fracture fluid cleanup process, a range of distinct simulation scenarios was meticulously designed for various DP levels; these scenarios are outlined in Table 3. For the purpose of this analysis, twelve key parameters deemed significant to the study were normalised onto a scale ranging from 0, representing the lower constraint, to 1, signifying the upper constraint. This established normalisation approach was implemented as it allows for a more robust and effective evaluation of the cleanup mechanisms through the application of response surface methodology (RSM).

2.2. Quantification of Production Impairment and Response Surface Modelling

The efficacy of the post-fracturing cleanup process is quantitatively assessed through the gas production loss (GPL) metric, expressed as a percentage. GPL is determined by evaluating the discrepancy between the cumulative gas production anticipated from an idealised, undamaged fracture system ($FGPT_{\text{clean}}$) and the production realised from the actual, potentially damaged fracture ($FGPT_{\text{unclean}}$). This difference is normalised relative to the idealised clean fracture production, as defined by the following relationship:

$$GPL = 100 \times \left[\frac{FGPT_{\text{clean}} - FGPT_{\text{unclean}}}{FGPT_{\text{clean}}} \right] \quad (5)$$

FGPT : Field gas cumulative production

It is widely recognised within the industry that achieving a perfectly ‘clean’ or entirely undamaged fracture condition subsequent to hydraulic fracturing operations presents significant technical challenges and may, in practice, be unattainable. Therefore, optimising field strategies to promote more effective fracture cleanup and consequently enhance well productivity is paramount. Such optimisation necessitates a thorough understanding of the intricate interplay between various operational and reservoir parameters and their impact on post-stimulation well performance. To facilitate direct comparisons across diverse scenarios, the GPL response is reported in this normalised format.

The sensitivity of gas production loss to twelve key influencing parameters, previously identified, is initially elucidated using tornado charts. This graphical sensitivity analysis indicates whether an increase in a specific parameter value exerts a positive influence on cleanup efficacy (resulting in reduced GPL and higher cumulative gas production) or a detrimental effect (leading to increased GPL and diminished cumulative production).

For a more comprehensive understanding of the complex, potentially non-linear relationships and interactions between multiple parameters and the primary response variable (GPL), response surface methodology (RSM) is employed. RSM provides a mathematical and statistical framework to model the functional relationship between several independent variables (x_1, x_2, \dots, x_n) and the output of interest (y or $f(x_i)$). The general form of the RSM polynomial utilised to approximate this relationship is given by

$$y = a_0 + \sum_{k=1}^n a_k x_k + \sum_{i=1}^n \sum_{j=i+1}^n a_{ij} x_i x_j + \sum_{l=1}^n a_l x_l^2 \quad (6)$$

Equation (6) encapsulates several potential model structures:

- **Linear Response Surface Model (LRSM):** Incorporates the constant (a_0) and linear terms ($\sum a_k x_k$).
- **Interaction Linear Response Surface Model (ILRSM):** Includes the LRSM terms plus the two-factor interaction terms ($\sum \sum a_{ij} x_i x_j$).
- **Pure Quadratic Response Surface Model (PQRSM):** Comprises the constant, linear, and pure quadratic terms ($\sum a_{ii} x_i^2$).
- **Full Quadratic Response Surface Model (FQRSM):** Encompasses all terms shown in Equation (6).

Within the scope of this investigation, both ILRSM and FQRSM models were developed to correlate GPL with the twelve pertinent factors identified. The dataset underpinning these models was generated using a Latin Hypercube Sampling (LHS) approach. The entire simulation workflow, including the necessary pre-processing steps, execution of reservoir simulations, and post-processing of results for the fracturing procedure, was automated through the development of dedicated Python 3.5.0 scripts.

While the Latin Hypercube Sampling (LHS) strategy in this study systematically investigated 12 influential parameters related to Kr, Pc, and matrix/fracture properties, we acknowledge that several additional factors known to affect fracture cleanup efficiency in field-scale conditions—such as fracture-network complexity (e.g., tortuosity, branching), proppant embedment, and thermal gradients—were not explicitly incorporated. These phenomena introduce important geomechanical, petrophysical, and thermodynamic interactions that can alter near-fracture flow regimes, damage mechanisms, and fluid mobility. Their exclusion was primarily carried out to constrain the dimensionality of the parametric space and isolate saturation-dependent effects. However, future extensions of this work will integrate these advanced parameters, potentially via coupled thermo-hydro-mechanical (THM) simulations and stochastic fracture-network generation to capture field-realistic geometries.

2.3. Quantification of Fracturing Fluid Recovery

Following the hydraulic fracturing treatment, a phase known as flowback occurs, during which a portion of the injected fracturing fluid (FF) is recovered at the surface. The volume of this recovered fluid can vary substantially, influenced significantly by the interplay of key operational parameters and the specific fracture-network design. The produced fluid stream typically consists of a mixture of the returned FF, native formation brine, and residual injected chemical additives.

Accurate quantification and prediction of the produced water volume are of critical importance. The management of produced FF presents considerable challenges in the development of unconventional gas formations, driven by stringent environmental regulations governing its handling and disposal, potential ecological impacts, and often limited or costly disposal options. These factors compel operators to continually evaluate and adapt their hydraulic fracturing and flowback management strategies.

To address the need for quantifying fluid recovery efficiency, a dimensionless metric, termed produced fracture fluid (PFF), has been introduced. This parameter serves as a secondary response metric in this study. PFF represents the proportion of the total injected FF volume recovered during the flowback period, relative to the total volume injected during the stimulation phase. It is calculated as follows:

$$\text{PFF} = 100 \times \left[\frac{\text{The volume of produced FF or simply Field water production}}{\text{Total FF injected at fracturing stage (FF injection stage)}} \right] \quad (7)$$

The influence of the same set of key parameters investigated for GPL was also examined with respect to their impact on PFF.

The synthetic heterogeneity models (Sets 37–39) were constructed using a truncated normal distribution to assign six rock types based on relative permeability and capillary pressure contrasts. While this statistical approach allows for systematic parametric sensitivity testing, we acknowledge that it does not fully replicate the complex spatial arrangements observed in real subsurface formations. In field applications, heterogeneity is often governed by depositional facies transitions, diagenetic cementation patterns, and natural fracture networks that influence pore structure and flow continuity. Future modelling efforts will incorporate geostatistical methods conditioned on geological depositional models or digital outcrop data to produce more geologically realistic heterogeneity structures.

2.4. Simulation Analysis Framework

The investigative methodology employed herein involved the systematic analysis of five distinct sets of simulations, each representing multi-fractured horizontal wells

(MFHWs). A total of 1000 individual simulation runs were conducted within each set. These simulation sets are summarised in Table 3. It is pertinent to note that while the fundamental reservoir dimensions were maintained consistently across all simulations within a given set, specific key parameters were systematically varied between the sets. These parameters included aspects of the capillary pressure (P_c) function (specifically, the entry pressure characteristic parameter, λ), the applied pressure drawdown during production, the intrinsic matrix permeability, and the total volume of fracturing fluid injected.

A base reference simulation set was established, incorporating the twelve pertinent factors varying within their default ranges, as delineated in Table 3 (indicated by checkmarks). Subsequent simulation sets were constructed by modifying the range of variation for one or more specific parameters relative to this base case. The nomenclature assigned to these additional sets was designed to reflect the nature and magnitude of the parameter range deviation compared to the reference set.

3. Results

3.1. Investigation of Base Reference Set and Weak Permeability Jail Effects via Modified Relative Permeability Curves in MFHW Simulations

To elucidate the influence of unconventional relative permeability characteristics, specifically the phenomenon termed the ‘weak permeability jail’, on fracturing fluid cleanup efficiency, a dedicated investigation employing numerical simulations of multi-fractured horizontal wells (MFHWs) was undertaken. This study focused on three newly configured simulation sets—Set 34, Set 35, and Set 36 (designated NF7 L600m)—alongside a base reference set for comparison.

In contrast to conventional relative permeability models where irreducible water saturation (S_{wirr}) and critical water saturation (S_{wc}) are often considered equal (e.g., 0.15), and critical gas saturation (S_{gc}) equals residual gas saturation (S_{gr}) (e.g., 0.1), the unconventional models incorporated distinct values to represent the weak permeability jail. For these three sets (Sets 34, 35, 36), S_{wirr} and S_{gr} were maintained at 0.15 and 0.1, respectively. However, the weak permeability jail effect was simulated by systematically shifting the relative permeability curves through adjustments to S_{wc} and S_{gc} . Specifically, for Sets 34, 35, and 36, the respective (S_{wc} , S_{gc}) pairs were assigned values of (40%, 30%), (45%, 35%), and (50%, 40%), as illustrated graphically (Figure 4). In these plots, both water and gas saturations are presented on a scale from 0 to 1, and relative permeability values are dimensionless.

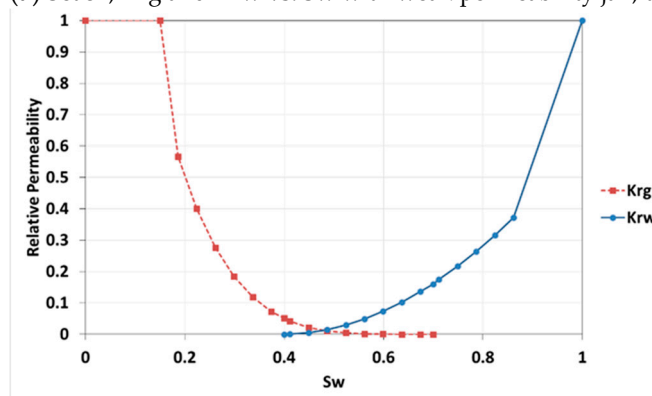
This parameterisation resulted in a progressively restricted saturation range for two-phase flow within Sets 34, 35, and 36, yielding mobile saturation windows of only 30%, 20%, and 10%, respectively. Examination of the relative permeability curves for these weak jail scenarios (Figure 4) revealed significantly reduced, albeit limited, fluid mobility within the ‘jail’ saturation region. A clear trend was observed wherein narrower two-phase regions (stronger jail effect) corresponded to lower relative permeability values for both the water and gas phases within that zone.

These three simulation sets featuring the weak permeability jail were evaluated comparatively against each other and against Set 30, which represented the scenario without this unconventional relative permeability feature. It is pertinent to note that, commencing with these simulation sets, unconventional capillary pressure (P_c) characteristics were also incorporated into the reservoir model. This concurrent inclusion allows for a more holistic assessment of cleanup efficiency under conditions reflecting both unconventional K_r and P_c behaviours.

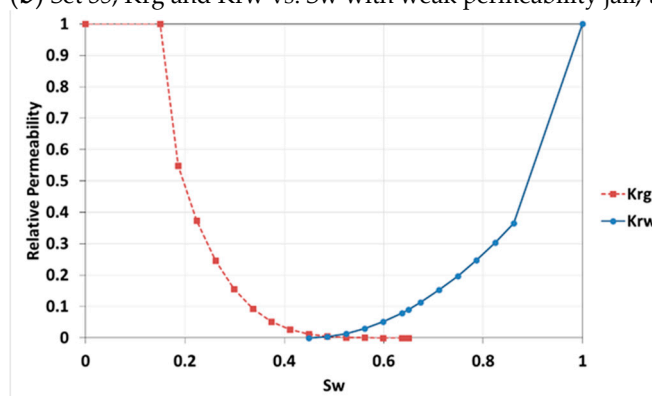
A comparative analysis of the Gas Production Lifetime (GPL) sensitivity, visualised through tornado charts for Sets 34, 35, and 36 (Figure 5a–c), relative to each other and to the baseline Set 30 (Figure 5d), highlights distinct parametric influences despite largely

consistent overall trends. The primary differentiator among Sets 34, 35, and 36 is the extent of the weak jail saturation region (30%, 20%, 10%). A notable observation is the diminished sensitivity of GPL to parameters governing capillary pressure (namely, interfacial tension—IFT—and the pore size distribution index— λ) as the intensity of the weak permeability jail effect increases. Essentially, a stronger jail effect correlates with reduced capillary influence on gas production outcomes.

(a) Set 34, K_{rg} and K_{rw} vs. S_w with weak permeability jail, two-phase 30%



(b) Set 35, K_{rg} and K_{rw} vs. S_w with weak permeability jail, two-phase 20%



(c) Set 36, K_{rg} and K_{rw} vs. S_w with weak permeability jail, two-phase 10%

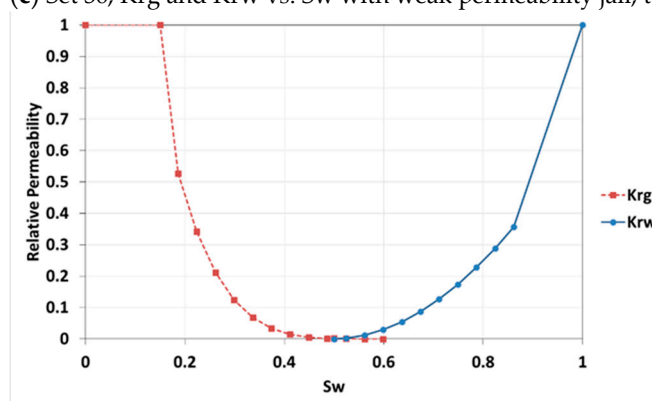
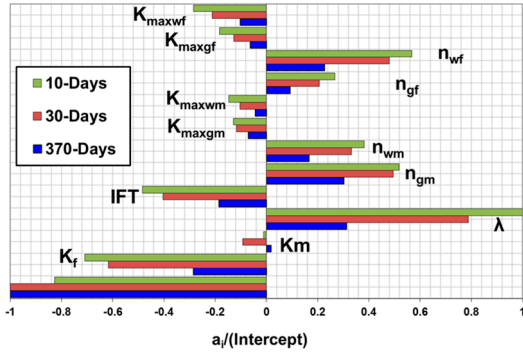


Figure 4. Relative permeability curves for weak jail effect. Note: All relative permeability (K_r) values are dimensionless, and water/gas saturations (S_w , S_g) are shown in normalised form, ranging from 0 to 1.

The ‘weak’ versus ‘strong’ permeability jail classifications used in this study—defined by 30%, 20%, and 10% two-phase saturation windows—are conceptual representations based on research-reported behaviour in tight formations exhibiting extreme pore-throat constriction. While direct MICP data were not used in this simulation set, the saturation window widths reflect values inferred from laboratory studies and core-scale mercury intrusion profiles that show sharply peaked pore-throat distributions in the nanometre range. Specifically,

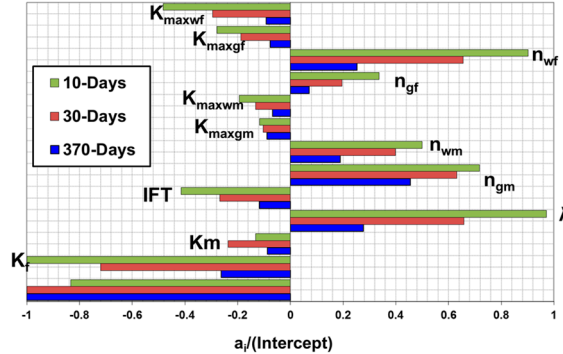
formations exhibiting narrow pore-throat size distributions tend to support shorter two-phase flow intervals due to rapid phase interference and snap-off. Future work will incorporate MICP data and digital rock-derived pore statistics to more rigorously constrain jail saturation definitions and strengthen their physical linkage to pore structure.

MFHW-Set 34 NF7-L600, 1000 runs, LHS, Weak Perm Jail, Two phase 30% GPL- LRSM



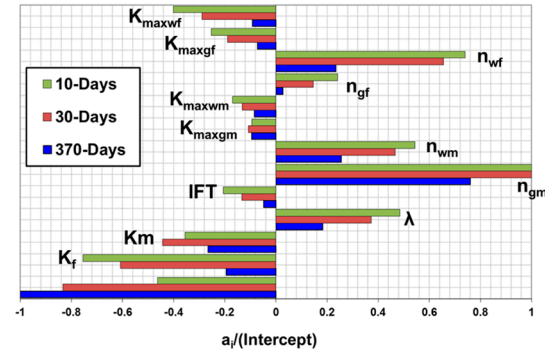
(a) Set 34 with weak permeability jail, two-phase 30%

MFHW-Set 35 NF7-L600, 1000 runs, LHS, Weak Perm Jail, Two Phase 20% GPL- LRSM



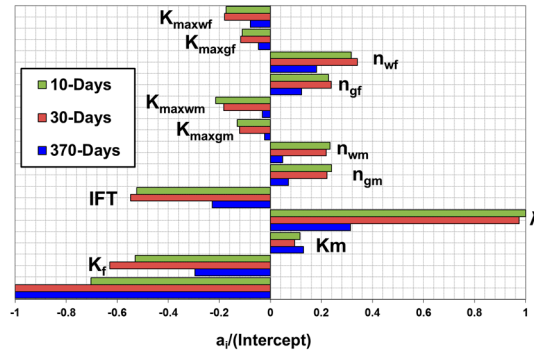
(b) Set 35 with weak permeability jail, two-phase 20%

MFHW-Set 36 NF7-L600, 1000 runs, LHS, Weak Perm Jail, Two Phase 10% GPL- LRSM



(c) Set 36 with weak permeability jail, two-phase 10%

MFHW-Set30 NF7-L600, 1000 runs, LHS, new Lambda (0.3 to 1.5), GPL- LRSM



(d) Base Reference Set 30

Figure 5. GPL tornado chart.

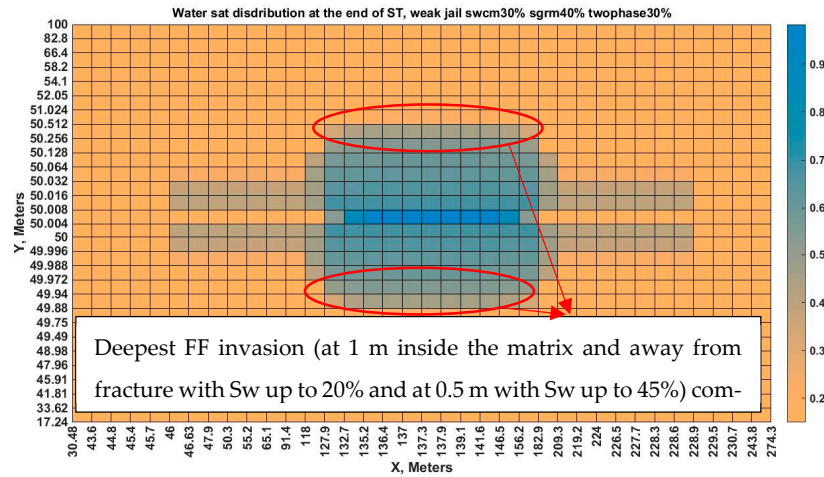
This observation aligns with a shift in the dominant role of matrix permeability (K_m). In the conventional case (Set 30), the secondary effect of K_m (its influence on P_c magnitude) appeared dominant. However, within the sets incorporating the weak permeability jail (Sets 34, 35, 36), the primary effect of K_m (its direct impact on fluid mobility) became preponderant. This transition is attributed to the progressive suppression of viscous forces as the permeability jail effect intensifies—moving from a 75% two-phase region in Set 30 down to 10% in Set 36.

Previous analysis (Set 30) suggested that stronger viscous forces facilitate deeper invasion of fracturing fluid (FF) into the matrix, leading to a more dispersed fluid distribution. This dispersion results in lower average water saturation (S_w) near the fracture face, thereby engaging higher capillary pressures and increasing fluid retention. Conversely, the weakened viscous forces associated with the permeability jail hinder deep FF invasion. This leads to FF accumulation at higher saturations closer to the fracture face. In these higher-saturation zones, capillary retention forces are lower, consequently promoting increased FF flowback during production. This mechanism explains the reduced importance of P_c -related parameters (IFT, λ , and the P_c -related aspect of K_m) in cleanup efficiency under stronger weak jail conditions and supports the observed shift in the primary influence of K_m from capillary effects to direct mobility control.

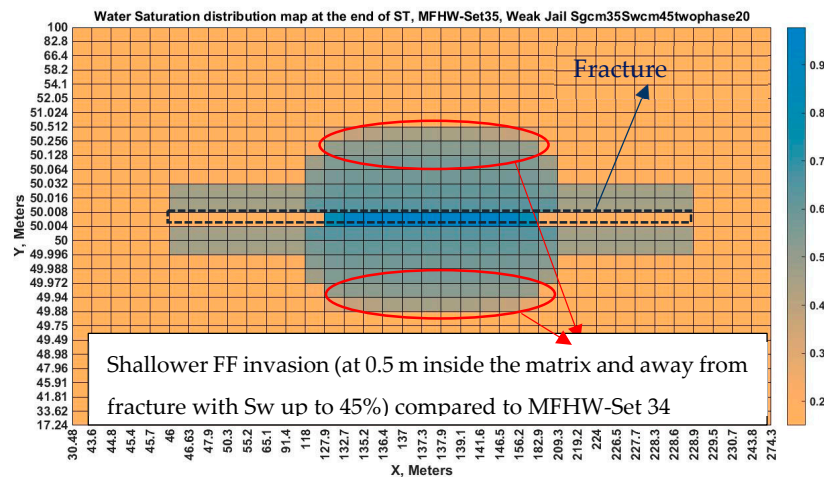
Visual confirmation of this behaviour is provided by saturation distribution maps at the cessation of the shut-in (soaking) period (Figure 6). These maps demonstrate that

intensifying the weak jail effect restricts the depth of FF invasion compared to scenarios with stronger viscous drive. Specifically, the deepest FF penetration is observed in Set 34 (weakest jail effect, 30% two-phase region), while the shallowest invasion occurs in Set 36 (strongest jail effect, 10% two-phase region).

(a) Set 34 with weak Perm jail, two-phase 30%



(b) Set 35 with weak Perm jail, two-phase 20%



(c) Set 36 with weak Perm jail, two-phase 10%

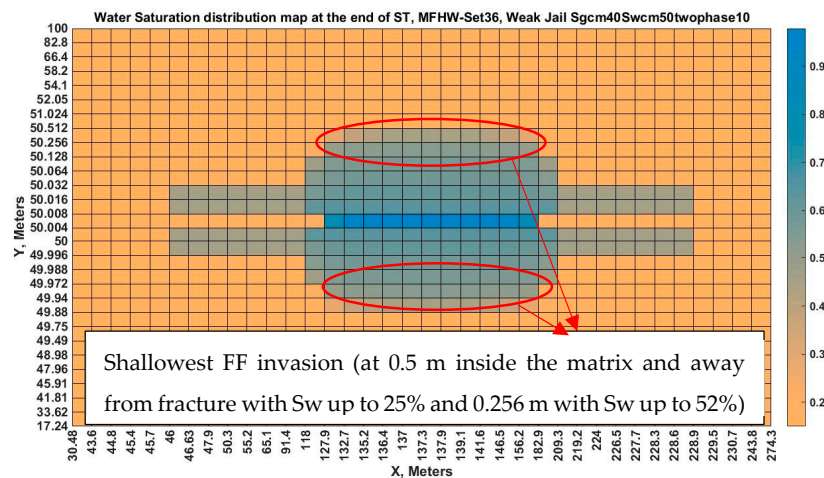


Figure 6. Saturation distribution map at the end of ST.

Furthermore, comparing the GPL tornado charts (Figure 5a–d) reveals that as the weak permeability jail effect is amplified, the sensitivity of cleanup efficiency to fluid mobility, particularly within the matrix, increases significantly. This heightened importance arises because matrix fluid transport becomes more rate-limiting under the constrained viscous conditions imposed by the jail effect. Simultaneously, the influence of fluid mobility within the fracture network also gains importance, likely due to the larger volumes of FF being produced back during the flowback phase under stronger jail conditions.

An analysis of cumulative frequency distributions for GPL via histogram charts (Figure 7), comparing Sets 36, 35, 34, and 30, indicates that a more pronounced weak jail effect correlates with slower cleanup dynamics. It was noted that as the weak jail effect intensifies, the volume of fracturing fluid recovered during flowback (PFF) tends to be larger (detailed in Figure 8a–c), and this higher fluid return corresponds to the observed GPL outcomes.

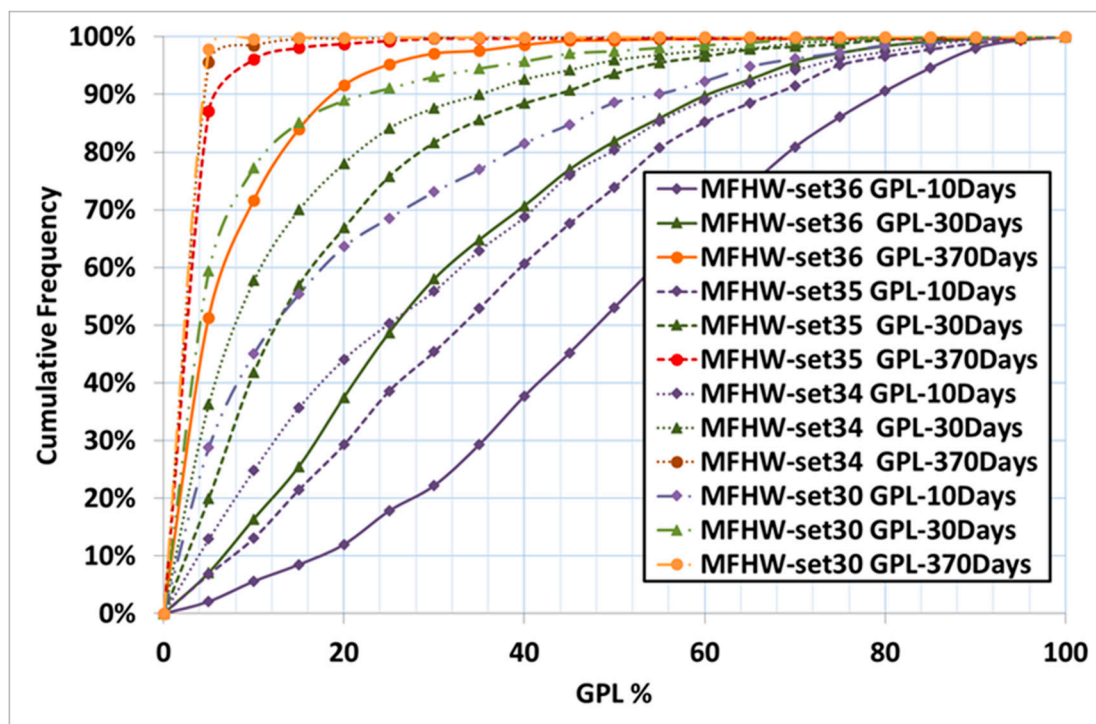
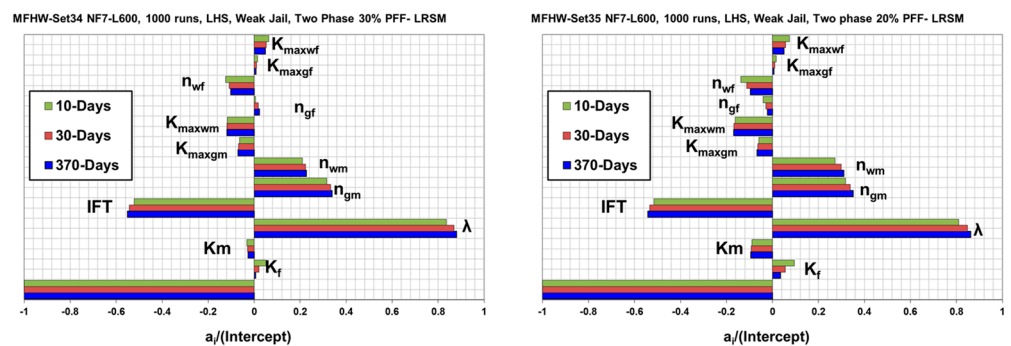
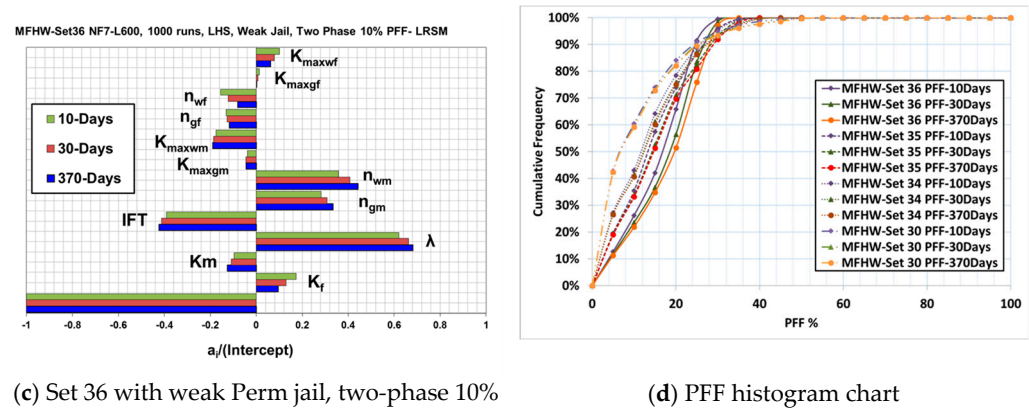


Figure 7. GPL histogram chart.



(a) Set 34 with weak Perm Jail, two-phase 30% (b) Set 35 with weak Perm jail, two-phase 20%

Figure 8. Cont.



(c) Set 36 with weak Perm jail, two-phase 10%

(d) PFF histogram chart

Figure 8. PFF tornado charts and histogram.

Consistent observations were made upon examining the tornado charts for the percentage of fracturing fluid recovered (PFF) across Sets 34, 35, and 36 (Figure 8a–c). These results reinforce the findings from the GPL analysis:

- Increasing the strength of the weak jail effect reduces the impact of capillary pressure on FF production.
- As the weak jail effect becomes more dominant, the influence of fluid mobility in both the matrix and the fracture system on FF flowback efficiency becomes more critical.

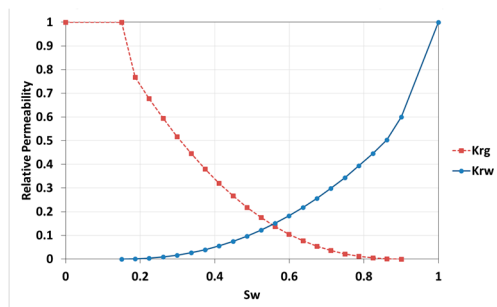
Finally, histogram comparisons of the cumulative frequency for PFF across the runs in Sets 36, 35, 34, and 30 (Figure 8d) confirm a direct relationship: stronger implementations of the weak permeability jail effect result in larger volumes of fracturing fluid being produced back.

3.2. Evaluation of Heterogeneous Reservoir Models Incorporating Strong and Weak Relative Permeability Constraints (Sets 37, 38, and 39)

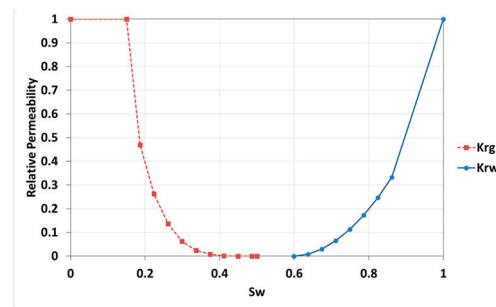
Further investigation into the impact of relative permeability (K_r) phenomena on multi-fractured horizontal well (MFHW) productivity necessitated the development of more complex, heterogeneous reservoir models. Preliminary assessments indicated that a homogeneous reservoir characterised solely by a ‘strong’ or ‘total’ permeability jail effect—where K_r curves are significantly shifted—results in negligible water or gas production following stimulation. Such a scenario, while theoretically illustrative of the extreme end-member, lacks practical relevance for typical unconventional tight/ultra-tight formations.

Recognising that actual reservoirs exhibit considerable heterogeneity, where hydraulic fractures inevitably intersect zones with diverse fluid flow characteristics, a more realistic approach was adopted. It is anticipated that fractures will encounter regions exhibiting total permeability jail, varying degrees of weak permeability jail, and conventional relative permeability behaviour. Figure 9a,b compare the relative permeability curves in a conventional rock and a rock with a total permeability jail effect with 10% total jail. In this study, the term ‘total permeability jail’ refers to a saturation range over which the relative permeability (K_r) for both gas and water phases is effectively zero ($K_r \approx 0$), indicating complete immobility of both phases. This representation captures an extreme case scenario where multiphase flow is entirely suppressed within the designated saturation interval, as illustrated in Figure 8b.

To capture this complexity and realistically evaluate the influence of these ‘jail’ zones on fracture cleanup efficiency, three new simulation sets were established: Set 37, Set 38, and Set 39. These sets utilised a consistent seven non-planar fracture configuration (NF7) with a 600 m length, comparable to the base reference simulation.



(a) Normal rock with conventional relative permeability



(b) Total permeability jail effect with 10% total jail

Figure 9. Relative permeability curves for (a) normal conventional rock & (b) total permeability jail effect with 10% total jail.

For these three heterogeneous investigations, an identical base grid model was employed but populated with differing spatial distributions of Kr properties. The reservoir volume was conceptualised as comprising six distinct rock type classes, each defined by a unique relative permeability function:

1. **Rock Type 1:** Represents regions experiencing a ‘total’ permeability jail effect. This was modelled by defining a 10% saturation range where multiphase flow is severely restricted. Specific parameters included an irreducible water saturation (S_{wirr}) of 0.15 and a residual gas saturation (S_{gr}) of 0.1, with critical water (S_{wc}) and gas (S_{gc}) saturations shifted significantly to 0.60 and 0.50, respectively (Figure 9b).
2. **Rock Type 2:** Simulates a ‘weak’ permeability jail effect across a 10% saturation window, consistent with Set 36 parameters ($S_{wirr} = 0.15$, $S_{gr} = 0.1$, $S_{wc} = 0.50$, $S_{gc} = 0.40$) (Figure 4c).
3. **Rock Type 3:** Incorporates a ‘weak’ permeability jail effect over a 20% saturation range, mirroring Set 35 ($S_{wirr} = 0.15$, $S_{gr} = 0.1$, $S_{wc} = 0.45$, $S_{gc} = 0.35$) (Figure 4b).
4. **Rock Type 4:** Represents a ‘weak’ permeability jail effect spanning a 30% saturation zone, as used in Set 34 ($S_{wirr} = 0.15$, $S_{gr} = 0.1$, $S_{wc} = 0.40$, $S_{gc} = 0.30$) (Figure 4a).
5. **Rock Type 5:** Characterises regions with conventional relative permeability behaviour, as defined in Set 30 ($S_{wirr} = 0.15$, $S_{gr} = 0.1$, $S_{wc} = 0.15$, $S_{gc} = 0.10$).
6. **Rock Type 6:** This designation was applied exclusively to the grid blocks representing the hydraulic fractures themselves. The relative permeability function within these elements was held constant ($S_{wirr} = 0.15$, $S_{gr} = 0.1$, $S_{wc} = 0.15$, $S_{gc} = 0.10$) across all simulation sets, irrespective of whether the matrix exhibited conventional or unconventional Kr behaviour.

The generation and visualisation of these heterogeneous reservoir models, with their varying Kr distributions, were accomplished using PETREL software [78,79]. A truncated normal distribution algorithm was implemented to randomly assign the different rock type properties throughout the reservoir grid. This statistical method ensures a realistic, yet bounded, distribution of properties.

As shown in Figure 10, the resultant compositions for each heterogeneous set were distinct:

- **Set 37 (Mixed 1):** Comprised approximately 10.1% Rock Type 1 (total jail), 23.9% Rock Type 2 (10% weak jail), 27.4% Rock Type 3 (20% weak jail), 26.7% Rock Type 4 (30% weak jail), and 12.0% Rock Type 5 (conventional).
- **Set 38 (Mixed 2):** Featured a higher proportion of jail-affected rock, with 17.1% Type 1, 31.7% Type 2, 26.3% Type 3, 18.6% Type 4, and 6.4% Type 5.
- **Set 39 (Mixed 3):** Represented the most pronounced overall jail effect, containing 21.3% Type 1, 36.5% Type 2, 24.7% Type 3, 13.4% Type 4, and 4.0% Type 5. Essentially,

the cumulative impact of permeability jail constraints intensified progressively from Set 37 through Set 38 to Set 39. Visual representations confirmed the distinct spatial arrangements of these rock types within each model.

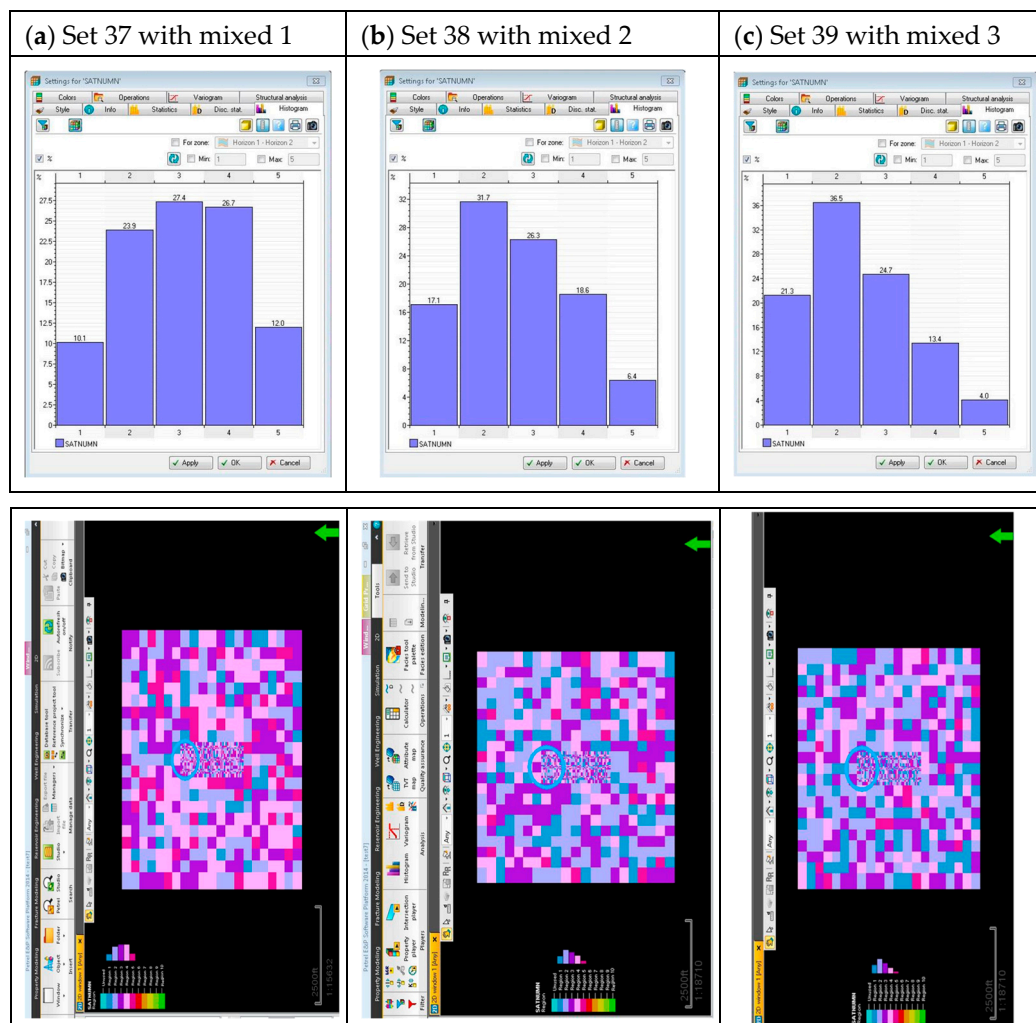


Figure 10. Rock type distribution in heterogeneous rocks. (The green arrow shows north direction, the blue circle shows the well.)

Sensitivity analyses, particularly gas production loss (GPL) tornado charts, for Sets 37, 38, and 39 are compared against the baseline conventional Kr model (Set 30) in Figure 11. These comparisons reinforced observations noted previously when analysing weak jail effects:

- As the prominence of the Kr jail effect increased across the heterogeneous sets, the relative impact of capillary pressure (P_c) on cleanup efficiency was observed to decrease.
- Concurrently, the influence of gas mobility, within both the matrix and the fracture network, became significantly more critical as the jail effect intensified. Consequently, the importance of matrix permeability (K_m), which directly governs mobility, was heightened in scenarios with more pronounced jail characteristics.

An examination of simulated fluid saturation distributions at the end of the stimulation phase offered valuable spatial insights. A simulation run using exclusively 'total jail' Kr curves (Rock Type 1) throughout the reservoir resulted in fracturing fluid (FF) being trapped entirely within the fractures and immediately adjacent matrix blocks, halting any production and effectively 'killing' the simulated well.

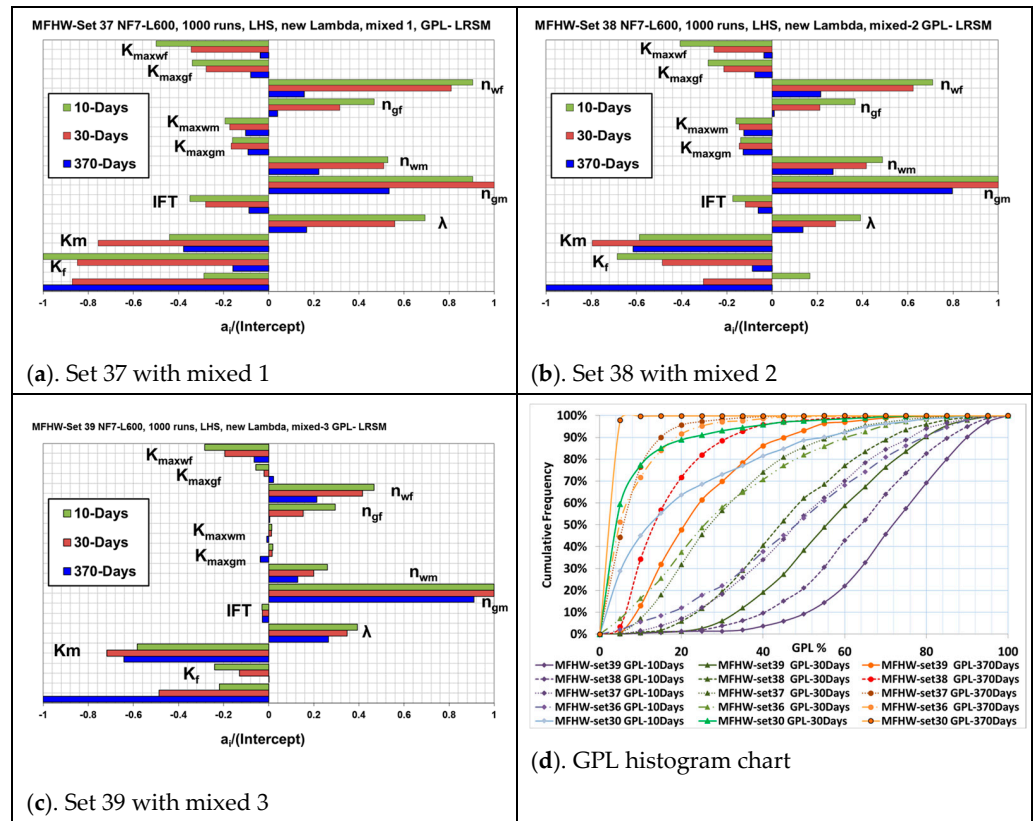


Figure 11. GPL tornado charts and histogram charts for heterogeneous rocks.

In contrast, the heterogeneous models (Sets 37, 38, 39) displayed notably asymmetrical saturation patterns resulting from the varied rock type distributions (Figure 12). A key observation was that within grid blocks characterised by the ‘total jail’ effect, FF invasion into the matrix via viscous forces was severely restricted. The primary mechanism for fluid movement into these matrix blocks appeared to be capillary imbibition (P_c), although its effectiveness seemed limited, potentially leading to lower water saturations (S_w) in neighbouring matrix cells not subject to the total jail.

Across all scenarios incorporating jail effects (homogeneous total jail and heterogeneous mixes), a consistent trend was observed: stronger jail effects led to shallower FF invasion depths into the matrix. This resulted in higher FF saturations remaining concentrated within the fractures and the near-fracture matrix region, a consequence of diminished viscous displacement forces.

Through a comparison of the heterogeneous saturation maps (Sets 37, 38, 39), it became evident that the ‘total jail’ zones act as significant barriers to viscous flow, forcing reliance on capillary forces for any matrix imbibition within those specific grid blocks.

Finally, Figure 13 compares cumulative frequency histograms for gas production loss (GPL) and percentage fracturing fluid recovery (PFF) across the various sets (including Sets 30, 36, 37, 38, 39), generally indicating that stronger overall permeability jail effects correlate with slower cleanup dynamics and higher ultimate fracturing fluid recovery percentages. Sensitivity analyses specific to PFF for Sets 37, 38, and 39 yielded results consistent with those observed in previous investigations focused solely on weak jail effects (Sets 34, 35, 36), lending further support to the identified controlling parameter relationships under these complex flow conditions.

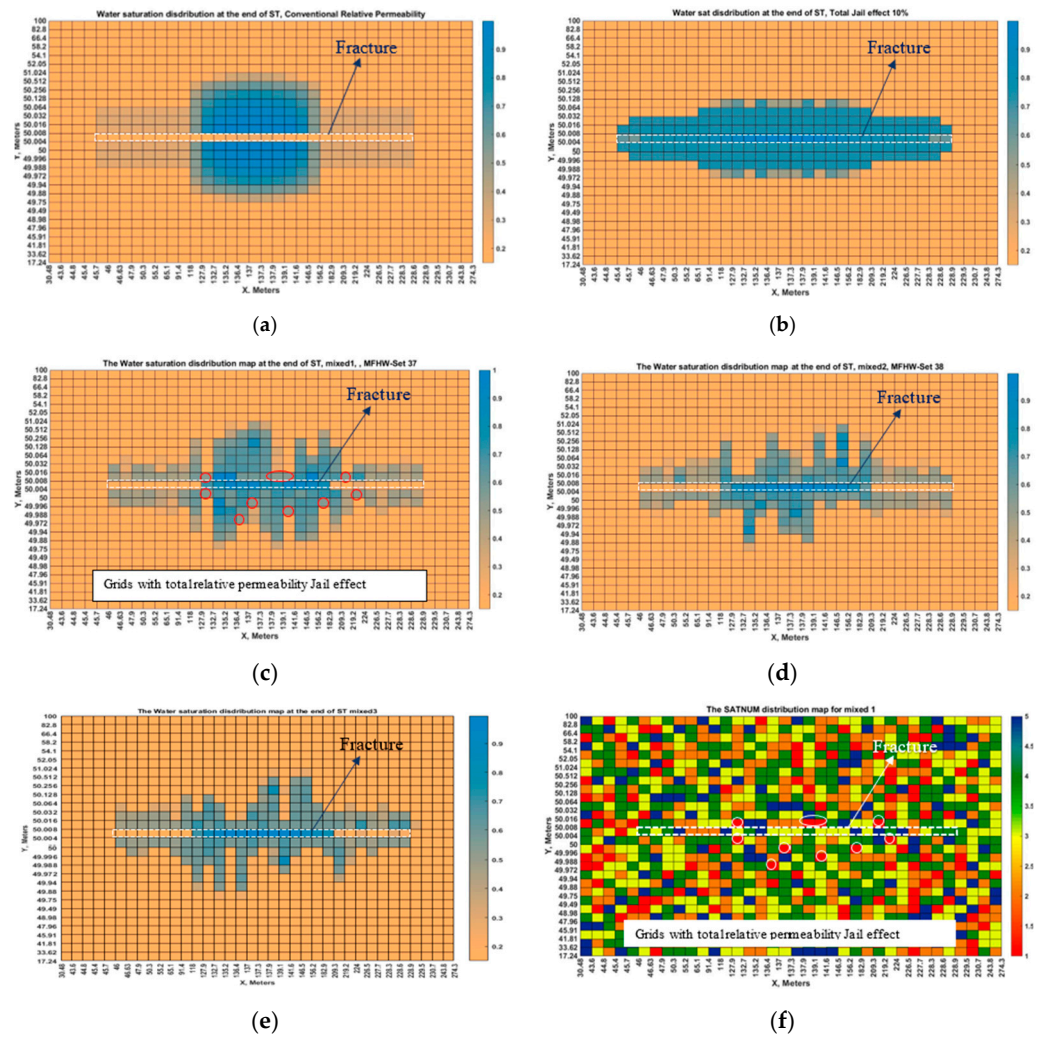


Figure 12. Saturation maps for homogeneous and heterogeneous rocks. (a) Rock with conventional relative permeability. (b) Total permeability jail effect with 10% total jail. (c) Set 37 with mixed 1. (d) Set 38 with mixed 2. (e) Set 39 with mixed 3. (f) SATNUM distribution map (run number 30) for Set 37 with mixed 1 (red circles are grids with total jail).

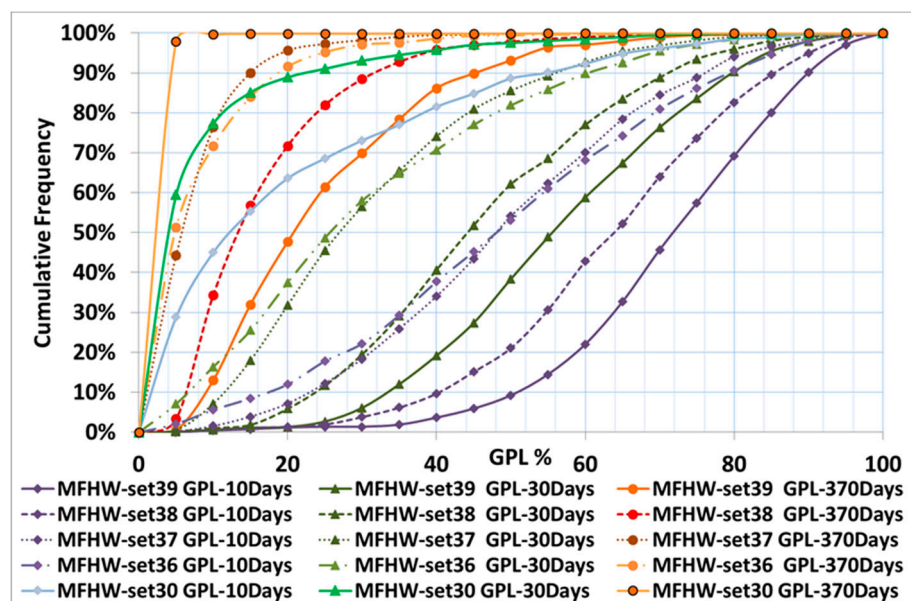


Figure 13. Cont.

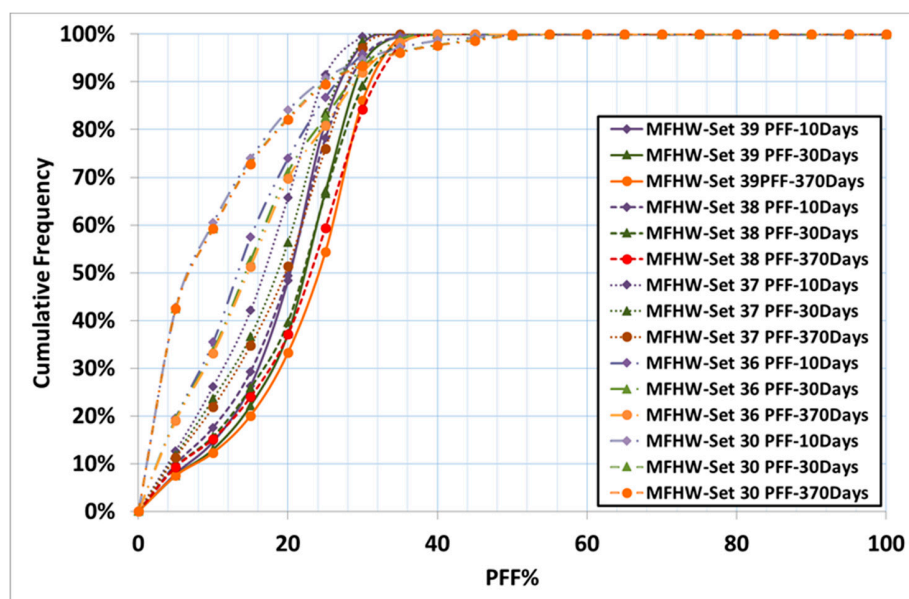


Figure 13. GPL histogram charts for GPL and PFF.

3.3. Investigation of Post-Fracturing Cleanup Dynamics in Heterogeneous Unconventional Reservoirs

The cleanup efficiency following hydraulic fracturing in multi-fractured horizontal wells (MFHWs) situated within heterogeneous reservoir formations was systematically evaluated. This investigation focused specifically on reservoirs characterised by unconventional capillary pressure (P_c) and relative permeability (K_r) functions, incorporating features like relative permeability jail effects. A series of numerical simulations were conducted, building upon a reference case exhibiting mixed wettability and significant permeability heterogeneity. Five distinct simulation sets were developed to explore the influence of key parameters on cleanup performance. These parameters included the injected fracturing fluid volume relative to the fracture volume (FVR), the duration of the shut-in period (ST), the applied pressure drawdown (DP) during production, and the range of matrix permeability (K_m).

3.3.1. Influence of Increased Fracturing Fluid Volume (FVR)

The analysis of a scenario with significantly increased injected fluid volume (FVR = 10 compared to the reference FVR = 2) revealed that the relative importance of governing parameters remained largely consistent. Matrix permeability and gas mobility within the matrix continued to exert the most substantial influence on cumulative gas production loss (GPL). However, the sensitivity to capillary pressure parameters and fracturing fluid mobility within the fracture network was diminished in the high-FVR case. Correspondingly, the influence of matrix and fracture permeability was less pronounced. The larger injected volume naturally resulted in higher initial fluid saturations within the fracture and matrix system, necessitating longer production times to achieve effective cleanup. Interestingly, the role of capillary pressure was observed to evolve over time; higher capillary forces (tending to retain fluid) appeared beneficial early in production, whereas lower capillary forces (promoting flowback) were advantageous during later production stages (e.g., after one year). This suggests that strategies to reduce capillary pressure, such as using interfacial tension (IFT)-reducing agents, might be more effective later in the well's life for enhancing gas recovery rather than solely focusing on initial cleanup. Overall, consistent with expectations, the larger injected volume led to a slower cleanup process.

3.3.2. Effect of Extended Shut-In Duration (ST)

Although the base case assumes a 2-day shut-in period, an extended shut-in sensitivity analysis was conducted to capture realistic field variations. Specifically, a 20-day shut-in scenario was simulated and compared to the baseline, in line with typical operational ranges (1–30 days) observed in tight gas and shale plays. While additional durations were not simulated in full, the observed trends between 2 and 20 days provide valuable insight into the dynamic impact of shut-in time on fluid imbibition, saturation redistribution, and subsequent flowback performance. Extending the shut-in period from a baseline of 2 days to 20 days amplified the significance of capillary pressure effects on gas production loss. This finding confirmed trends previously observed in studies involving both single-fracture and MFHW models, even when using conventional flow functions. The extended shut-in duration provided more time for the spontaneous imbibition of the fracturing fluid from the fractures deeper into the surrounding matrix rock. This process resulted in a more dispersed fluid saturation profile within the matrix system and, consequently, lower initial fluid saturation within the fractures themselves at the onset of production flowback. While this redistribution of fluid led to faster initial cleanup rates (as less mobile fluid was immediately present in the high-conductivity fractures), the total volume of fracturing fluid ultimately recovered (PFF) was observed to be lower. This reduction in recovery is attributed to the increased fluid retention within the matrix pores caused by the prolonged imbibition period, making subsequent extraction more challenging.

3.3.3. Impact of Production Pressure Drawdown (DP) Variation

Variations in the applied production pressure drawdown also yielded significant insights into the interplay between viscous and capillary forces during cleanup. When the drawdown was substantially reduced (e.g., by a factor of ten, to 100 psi from a 1000 psi base), the influence of capillary pressure effects became considerably more pronounced relative to viscous forces. Furthermore, the parameters defining matrix relative permeability curves (specifically endpoints and Corey exponents) gained importance in controlling the overall cleanup. This observation highlights the dominance of matrix-to-fracture fluid transfer under low-drawdown conditions, where the pressure gradient driving flow is weaker. Consequently, under low drawdown, cleanup was observed to be slower, and overall fluid recovery was reduced. Conversely, increasing the drawdown significantly (e.g., fourfold, to 4000 psi) diminished the relative importance of capillary pressure. In this high-drawdown scenario, matrix flow characteristics became slightly less critical, suggesting a greater emphasis on the efficiency of fluid transport within the fracture network towards the wellbore. This resulted in faster cleanup kinetics and higher cumulative fluid recovery. These findings regarding the influence of drawdown levels align consistently with previous investigations across different model types.

While this study focused primarily on static drawdown levels and fixed fracture conductivities, we acknowledge that stress-sensitive permeability and cyclic loading effects can significantly influence long-term fracture performance. Under variable drawdown conditions, fracture conductivity may degrade over time due to proppant crushing, embedment, and fracture face asperity closure—phenomena well documented in tight gas fields. These time-dependent geomechanical interactions may intensify permeability jail conditions by further reducing near-fracture mobility. Although not explicitly modelled here, these effects merit inclusion in future coupled geomechanical–flow simulations to improve the representation of dynamic cleanup impairment.

3.3.4. Consequences of Reduced Matrix Permeability (Km Range)

Finally, the impact of inherent reservoir quality was examined by simulating scenarios within tighter formations. This was achieved by reducing the range of matrix permeability assumed in the heterogeneous model by an order of magnitude (from 1 to 100 μD down to 0.1 to 10 μD). In these tighter formations, the parameters governing gas mobility within the matrix became even more critical determinants of cleanup efficiency. This is an expected outcome, as fluid transport through lower-permeability matrix material inherently becomes more restricted and thus more influential in the overall system performance. A noteworthy observation specific to this low-permeability scenario was the time-dependent nature of the sensitivity to the interfacial tension (IFT) coefficient, particularly evident at later production times (e.g., 365 days). Similarly to the findings in the high-FVR case, detailed analysis of the capillary pressure behaviour indicated that while higher capillary pressure (promoting fluid retention) was beneficial for minimising gas production loss initially, lower capillary pressure (facilitating flowback, potentially achievable via IFT reduction) favoured better cleanup and reduced gas production loss at later production times. As anticipated from fundamental fluid flow principles, simulating the tighter rock resulted in significantly slower overall cleanup dynamics compared to the base reference case with higher matrix permeability.

It is acknowledged that suggesting that stronger jail effects necessitate higher matrix permeability may appear counterintuitive in the context of ultra-tight formations, where inherent matrix permeability often lies well below 100 μD . In this study, the observation stems from a modelling standpoint: in scenarios with severely suppressed relative permeability ($K_r \approx 0$) in the near-fracture region, even marginal increases in matrix permeability can substantially aid in restoring hydraulic continuity and enabling gas mobilisation into the fracture. From a practical standpoint, however, the enhancement of matrix–fracture connectivity must often rely on stimulation techniques rather than inherent permeability. Approaches such as matrix acidizing (to dissolve carbonate cements or enlarge microfractures), surfactant- and solvent-based flowback aids (to alter wettability and reduce IFT), or even CO_2 -based huff-and-puff injection strategies may mitigate near-fracture trapping and improve flowback. We have now added a clarification in the conclusion to reflect this distinction between modelling implications and field applicability.

3.3.5. Concluding Remarks of Section 3.3

In summary, these simulation studies underscore the complex interplay between operational parameters selected during well completion and initial production (such as injected fluid volume, shut-in time, and drawdown strategy) and the inherent characteristics of the reservoir (including heterogeneity, permeability range, and unconventional capillary/relative permeability behaviour) in dictating post-fracturing cleanup efficiency in MFHWs. Matrix properties, particularly permeability and the associated gas mobility, consistently emerge as critical factors influencing gas production loss. Capillary pressure effects are demonstrably significant, but their relative importance and even the direction of their optimal influence (whether high or low P_c is preferable) are strongly modulated by the applied drawdown and the duration of any shut-in period. Furthermore, the ideal capillary pressure state can evolve over the production life of the well. This temporal evolution suggests that interventions aimed at modifying capillary forces, such as the application of IFT-reducing chemical treatments, might require careful consideration regarding the timing of their application to maximise benefits for late-life production enhancement rather than solely focusing on immediate post-fracturing fluid recovery.

It is acknowledged that under high-rate gas production conditions, non-Darcy flow effects—typically captured via Forchheimer-type corrections—can become significant

within the fracture domain. These inertial effects introduce additional pressure losses and may compound permeability jail conditions by further impeding gas mobility near the fracture face. While the current study focused on Darcy-based formulations to isolate capillary- and saturation-dependent effects, future simulations should incorporate non-Darcy flow models to more accurately represent gas dynamics in high-rate production scenarios, particularly in stimulated fracture networks.

While the current study focuses on the physical and operational parameters affecting post-fracture fluid cleanup, the role of fracturing fluid chemistry—particularly surfactant-induced interfacial tension (IFT) reduction and clay swelling inhibition—is acknowledged as a critical factor influencing capillary trapping and permeability jail severity. Additives such as surfactants and mutual solvents can lower capillary entry pressures and alter wettability, enhancing fluid mobility during flowback. Additionally, chemical interactions such as clay swelling or fines migration may exacerbate near-fracture damage. Although these chemical effects were not explicitly modelled here, their incorporation into future simulation frameworks will allow for more realistic assessments of fluid–rock interactions and the efficacy of engineered fluid systems in mitigating cleanup impairment.

4. Conclusions

To advance the understanding of hydraulic fracturing treatments in tight and ultra-tight gas reservoirs, this research systematically extended previous analyses to capture the intricate impacts of unconventional capillary pressure (P_c) and relative permeability (K_r) characteristics on the cleanup performance of multiple-fractured horizontal wells (MFHWs). Building on the foundations established in earlier phases, a comprehensive investigation into unconventional K_r behaviours, particularly focusing on the permeability jail phenomenon, was undertaken. Furthermore, a novel dimensionless parameter, comparable to gas production loss (GPL), was formulated to quantify the influence of key operational and reservoir parameters on the production of fracturing fluid (FF), a critical aspect in optimising hydraulic fracturing efficiency in unconventional systems.

The findings corroborate previous experimental studies, providing a more reliable basis for modelling fluid invasion and displacement during post-fracture flowback.

A detailed examination of K_r behaviour revealed the critical influence of the permeability jail effect, wherein both gas and water exhibit negligible relative permeability over a specific saturation range. Although laboratory confirmation of this phenomenon remains pending, its strong theoretical and numerical support underscores its importance in understanding unconventional flow dynamics. The permeability jail was attributed to the combined effects of complex pore geometries, high capillary entry pressures, and confinement-induced pore-throat constriction, all of which significantly impair phase mobility relative to conventional formations.

To numerically capture these behaviours, an advanced adaptation of the Corey-type model was employed, introducing a substantial divergence between critical saturation (denoting phase mobilisation in the drainage path) and trap endpoint saturation (reflecting residual immobilisation during imbibition). This approach facilitated the representation of both weak permeability jail cases—where limited mobility persists—and strong or total jail scenarios—where complete immobilisation occurs within a saturation band. Simulations incorporating weak jail conditions with varying two-phase flow region widths (e.g., 30%, 20%, 10%) provided new insights into how saturation-dependent mobility impairments influence fracture fluid recovery and gas production.

The analysis of MFHW simulation sets integrating unconventional K_r and P_c characteristics led to several pivotal findings:

- **Diminishing Role of Capillary Pressure:** As the strength of the permeability jail increased, the influence of P_c on cleanup efficiency and FF flowback diminished markedly. In the presence of a pronounced jail effect, the intrinsic mobility limitations imposed by K_r became the dominant factor controlling fluid behaviour, overshadowing the traditional capillary force-driven mechanisms.
- **Enhanced Importance of Fluid Mobility:** With the emergence of stronger permeability jail effects, the role of fluid mobility within both the matrix and the fracture grew in significance. Particularly, the dependency on matrix permeability (K_m) shifted predominantly towards enhancing fluid displacement capabilities, as opposed to its traditional influence on capillary equilibrium. Under pronounced jail conditions, higher K_m values consistently facilitated improved cleanup and FF production, suggesting that enhancing matrix connectivity is critical when permeability barriers dominate.
- **Slower Cleanup Dynamics:** Stronger jail effects were consistently associated with slower cleanup rates. The pronounced suppression of multiphase flow within the jail saturation window delayed fracturing fluid recovery and prolonged gas production ramp-up, underscoring the operational challenges inherent to these formations.

Further extensions of this study incorporated heterogeneous reservoir models featuring spatially distributed zones of total permeability jail, weak jail, and conventional K_r characteristics, combined with unconventional P_c profiles. Variations in operational parameters such as the fluid volume ratio (FVR), drawdown pressure (DP), shut-in time (ST), and matrix permeability range were systematically tested. Despite the added complexity of heterogeneity, the fundamental trends observed under homogeneous conditions persisted: a higher FVR led to delayed cleanup; increased DP generally expedited cleanup except under strong P_c dominance; longer ST promoted early-time cleanup through enhanced imbibition; and lower K_m resulted in slower recovery. These consistencies reinforce the robustness of the conceptual frameworks developed herein across a range of practical reservoir conditions.

This study's outcomes provide important advancements in the understanding of post-fracture flowback in ultra-tight formations. Notably, the permeability jail concept emerges as a unifying explanation for many of the flow anomalies observed in field operations, offering predictive insights into flowback efficiency and gas production performance. The refinement of P_c models and the successful adaptation of Corey-type K_r curves to accommodate jail effects represent significant methodological contributions, bridging the gap between laboratory characterisation, numerical simulation, and field-scale application.

Overall, it is demonstrated that as the severity of the permeability jail increases, the control over hydraulic fracture cleanup shifts fundamentally from capillary-dominated mechanisms to mobility-constrained flow regimes. This shift necessitates a rethinking of stimulation design and flowback management strategies, placing greater emphasis on preserving matrix and fracture conductivity, optimising shut-in protocols, and tailoring drawdown profiles to the mobility limitations of the system. These insights offer critical guidance for engineers and operators engaged in the development of unconventional gas resources, supporting the design of more efficient, resilient, and economically viable production strategies in the most challenging reservoir environments.

We acknowledge the importance of field data in reinforcing simulation insights and enhancing model credibility. While this study focused on controlled parametric analysis using synthetic data calibrated against core-derived K_r/P_c behaviour, we plan to incorporate production logs and flowback data from field-scale MFHW projects in future phases. Preliminary benchmarking of simulation outputs against anonymised operator-supplied datasets from tight gas wells in North America has shown encouraging trends—particularly regarding the influence of shut-in time and drawdown on cleanup dynamics. However, full

integration of production log data, tracer diagnostics, or rate-transient analysis is required to comprehensively validate permeability field behaviour at the field scale.

Author Contributions: Conceptualization, H.R.N. and M.J.; methodology, H.R.N.; software, H.R.N.; validation, H.R.N.; formal analysis, H.R.N.; investigation, H.R.N. and M.J.; resources, H.R.N. and M.J.; data curation, H.R.N.; writing—original draft preparation, H.R.N.; writing—review and editing, H.R.N. and M.J.; visualization, H.R.N.; supervision, M.J.; project administration, M.J.; funding acquisition, M.J. All authors have read and agreed to the published version of the manuscript.

Funding: This research received no external funding.

Data Availability Statement: Data supporting reported results can be found at: <https://www.ros.hw.ac.uk/handle/10399/3256>.

Conflicts of Interest: The authors declare no conflict of interest.

Nomenclature

Nomenclature:

a_i	coefficients of the equation
B_o	oil formation factor
h	reservoir thickness
J	productivity index
k	absolute reservoir permeability
k_v	vertical permeability
k_h	horizontal permeability
K_r	relative permeability
K_{max}	end point of the Corey relative permeability curve
K_{mr}	matrix permeability ratio: i.e., if $K_{mr} = 10$, the K_m variation range is reduced by a factor of 10
L	length
M	mobility
n_g	exponent of the gas Corey relative permeability curve
n_w	exponent of the water Corey relative permeability curve
N_f	number of fractures
P	pressure
P_c	capillary pressure
P_d	threshold pressure
q	flow rate
r	radius
S_w	water saturation
S_{wi}	initial water saturation
S_{wir}	irreducible water saturation
S_{wc}	critical water saturation
S_{gr}	residual gas saturation
S_{gc}	critical gas saturation
W_f	fracture width
X_f	half-length of the fracture
x	x direction
y	y direction
z	z direction

Greek Letters:

φ	porosity
μ	viscosity
ρ	density
λ	pore size distribution index

σ interfacial tension

Subscript:

ave average
 bhp bottom-hole pressure
 c condensate
 dew dew point
 f fracture
 g gas
 h horizontal
 HW horizontal well
 i an index
 j an index
 m matrix
 o oil
 r residual
 x x direction
 y y direction
 w refers to wellbore

Abbreviations:

AD% absolute deviation (percentage)
 AAD% average absolute percentage deviation
 CCE constant composition expansion
 CPU computer processing unit
 CVD constant volume depletion
 DP pressure drawdown
 Dra drainage
 EOS equation of state
 FF fracture fluid
 FFPT total fracturing fluid production
 FFR fracture fluid residue
 FFV fracture fluid volume
 FFS full factorial sampling
 FGPT total cumulative gas production
 FVR ratio of injected fracture fluid to fracture volume
 FQRSM full quadratic response surface model
 GCR gas condensate research group
 GPL gas production loss
 GPR gas production rate
 HF hydraulic fracturing
 HFW hydraulically fractured well
 HW horizontal well
 HWU Heriot-Watt University
 IFT interfacial tension
 Imb imbibition
 IPE Institute of Petroleum Engineering
 ILRSM interactive linear response surface model
 LGR local grid refinement.
 LHS Latin hypercube sampling
 LRM linear response surface model
 MEPO MEPO Multiple Realization Optimizer software
 MFHW multiple-fractured horizontal well
 OH open-hole
 PFF produced fracturing fluid
 PR productivity ratio

PR3	3-parameter Peng–Robinson equation of state
PQRSM	pure quadratic response surface model
Python	Python programming language
RMSE	root mean square error
RSM	response surface model
SFVW	single-fractured vertical well
SL	single layer
TL	two layer
SRV	stimulated reservoir volume
ST	shut-in/soaking time
TGP	total gas production
VW	vertical well
1-D	one-dimensional
2-D	two-dimensional
3-D	three-dimensional

References

- Dong, Z.; Holditch, S.A.; McVay, D.; Ayers, W.B. Global Unconventional Gas Resource Assessments. *Soc. Pet. Eng.* **2011**, *4*, 222–234. [[CrossRef](#)]
- Rushing, J.A.; Newsham, K.E.; Blasingame, T.A. Rock Typing: Keys to Understanding Productivity in Tight Gas Sands. In Proceedings of the SPE Unconventional Reservoirs Conference, Keystone, CO, USA, 10–12 February 2008; pp. 72–102. [[CrossRef](#)]
- Byrnes, A.P. Issues with gas relative permeability in low-permeability sandstones. In *Understanding, Exploring, and Developing Tight-Gas Sands—2005 Vail Hedberg Conference: AAPG Hedberg Series*; American Association of Petroleum Geologists: Tulsa, OK, USA, 2005; Volume 3, pp. 63–76.
- Byrnes, A.P. Reservoir characteristics of low-permeability sandstones in the Rocky Mountains. *Mt. Geol.* **1996**, *34*, 39–48.
- Byrnes, A.P. Aspects of permeability, capillary pressure, and relative permeability properties and distribution in low-permeability rocks important to evaluation, damage, and stimulation. In Proceedings of the Rocky Mountain Association of Geologists—Petroleum Systems and Reservoirs of Southwest Wyoming Symposium, Denver, CO, USA, 19 September 2003; p. 12.
- Cluff, R.M.; Byrnes, A.P. Relative Permeability in Tight Gas Sandstone Reservoirs—The “Permeability Jail” Model. In Proceedings of the SPWLA 51st Annual Logging Symposium, Perth, Australia, 19–24 June 2010; Society of Petrophysicists and Well-Log Analysts: Houston, TX, USA, 2010.
- Byrnes, A.P. *Role of Induced and Natural Imbibition in frac Fluid Transport and Fate in Gas Shales. For the Hydraulic Fracturing Study: Fate and Transport*; U.S. Environmental Protection Agency: Washington, DC, USA, 2011; p. 70.
- Byrnes, A.P.; Zhang, S.; Canter, L.; Sonnenfeld, M.D. Application of integrated core and 3D image rock physics to characterize Niobrara chalk properties including relative permeability with bound water effect. In Proceedings of the Unconventional Resources Technology Conference, Austin, TX, USA, 24–26 July 2017; Society of Exploration Geophysicists, American Association of Petroleum Geologists, Society of Petroleum Engineers: Tulsa, OK, USA, 2017; pp. 1584–1603.
- Holditch, S.A. Factors Affecting Water Blocking and Gas Flow From Hydraulically Fractured Gas Wells. *J. Pet. Technol.* **1979**, *31*, 1515–1524. [[CrossRef](#)]
- Gdanski, R.D.; Weaver, J.; Slabaugh, B.; Walters, H.; Parker, M. Fracture Face Damage—It Matters. In Proceedings of the SPE European Formation Damage Conference, Sheveningen, The Netherlands, 25–27 May 2005; p. 94649.
- Nasriani, H.R.; Jamiolahmady, M. Flowback cleanup mechanisms of post-hydraulic fracturing in unconventional natural gas reservoirs. *J. Nat. Gas. Sci. Eng.* **2019**, *66*, 316–342. [[CrossRef](#)]
- Nasriani, H.R.; Jamiolahmady, M. Maximizing fracture productivity in unconventional fields; analysis of post hydraulic fracturing flowback cleanup. *J. Nat. Gas. Sci. Eng.* **2018**, *52*, 529–548. [[CrossRef](#)]
- Nasriani, H.R.; Jamiolahmady, M. Optimising Flowback Strategies in Unconventional Reservoirs: The Critical Role of Capillary Forces and Fluid Dynamics. *Energies* **2024**, *17*, 5822. [[CrossRef](#)]
- Nasriani, H.R.; Jamiolahmady, M.; Saif, T.; Sánchez, J. A systematic investigation into the flowback cleanup of hydraulic-fractured wells in unconventional gas plays. *Int. J. Coal. Geol.* **2018**, *193*, 46–60. [[CrossRef](#)]
- MoradiDowlatabad, M.; Nasriani, H.R.; Rashidi, F.; Movahedi, M. Modelling and performance evaluation of gas condensate reservoirs-inclusion of porous media properties. In Proceedings of the 79th EAGE Conference and Exhibition 2017, Paris, France, 12–15 June 2017.

16. Jamiolahmady, M.; Alajmi, E.; Nasriani, H.R.; Ghahri, P.; Pichestapong, K. A Thorough Investigation of Clean-up Efficiency of Hydraulic Fractured Wells Using Statistical Approaches. In Proceedings of the SPE Annual Technical Conference and Exhibition, Amsterdam, The Netherlands, 27–29 October 2014. [CrossRef]
17. Society of Petroleum Engineers. *Engineers Glossary of Terms Used in Petroleum Reserves/Resources Definitions*; Society of Petroleum Engineers: Richardson, TX, USA, 2005. Available online: <https://www.spe.org/en/industry/reserves/> (accessed on 19 June 2016).
18. Yu, H.; Xu, H.; Fan, J.; Zhu, Y.B.; Wang, F.; Wu, H. Transport of Shale Gas in Microporous/Nanoporous Media: Molecular to Pore-Scale Simulations. *Energy Fuels* **2021**, *35*, 911–943. [CrossRef]
19. Zhao, Y.; Luo, M.; Liu, L.; Wu, J.; Chen, M.; Zhang, L. Molecular dynamics simulations of shale gas transport in rough nanopores. *J. Pet. Sci. Eng.* **2022**, *217*, 110884. [CrossRef]
20. Mo, F.; Du, Z.; Peng, X.; Liang, B. Pore-scale modeling of gas-water flow in permeability jail of tight sandstones. *J. Porous Media* **2019**, *22*, 1273–1288. [CrossRef]
21. Mo, F.; Qi, Z.; Yan, W.; Huang, X.; Fang, F.; Li, J.; Lei, D. Reservoir simulation study on the permeability jail's effect during tight gas production. *J. Porous Media* **2021**, *24*, 77–95. [CrossRef]
22. Mo, F.; Du, Z.; Peng, X.; Liang, B.; Tang, Y.; Yue, P. Analysis of pressure-dependent relative permeability in permeability jail of tight gas reservoirs and its influence on tight gas production. *J. Porous Media* **2019**, *22*, 1667–1683. [CrossRef]
23. Ojha, S.P.; Misra, S.; Tinni, A.; Sondergeld, C.; Rai, C. Relative permeability estimates for Wolfcamp and Eagle Ford shale samples from oil, gas and condensate windows using adsorption-desorption measurements. *Fuel* **2017**, *208*, 52–64. [CrossRef]
24. Agostini, F.; Egermann, P.; Jcannin, L.; Portier, E.; Skoczylas, F.; Wang, Y. Loading effects on gas relative permeability of a low-permeability sandstone. *Petrophysics* **2019**, *60*, 326–334. [CrossRef]
25. Fan, J.; Zhou, H.; Liu, S.; Liu, K. Gas-water two phases flow characterization and its influencing factors in low permeability tight sandstone. In Proceedings of the Unconventional Resources Technology Conference 2013, URTC 2013, Denver, CO, USA, 12–14 August 2013. [CrossRef]
26. Shanley, K.W.; Cluff, R.M.; Robinson, J.W. Factors controlling prolific gas production from low-permeability sandstone reservoirs: Implications for resource assessment, prospect development, and risk analysis. *Am. Assoc. Pet. Geol. Bull.* **2004**, *88*, 1083–1121.
27. Zhang, J.; Li, X.; Shen, W.; Gao, S.; Liu, H.; Ye, L.; Fang, F. Study of the Effect of Movable Water Saturation on Gas Production in Tight Sandstone Gas Reservoirs. *Energies* **2020**, *13*, 4645. [CrossRef]
28. Walls, J.D.; Nur, A.M.; Bourbie, T. Effects of pressure and partial water saturation on gas permeability in tight sands: Experimental results. *J. Pet. Technol.* **1982**, *34*, 930–936.
29. Lis-śledziona, A.; Stadtmüller, M. Determining irreducible water saturation based on well log data and laboratory measurements. *Nafta-Gaz* **2019**, *75*, 239–246. [CrossRef]
30. Miao, J.; Zhong, C. Dynamic Variation of Water Saturation and Its Effect on Aqueous Phase Trapping Damage during Tight Sandstone Gas Well Production. *ACS Omega* **2021**, *6*, 5166–5175. [CrossRef]
31. Gdanski, R.D.; Walters, H.G. Impact of Fracture Conductivity and Matrix Relative Permeability on Load Recovery. In Proceedings of the SPE Annual Technical Conference and Exhibition, Florence, Italy, 19–22 September 2010; Society of Petroleum Engineers: Dallas, TX, USA, 2010. [CrossRef]
32. Lai, F.P.; Li, Z.P.; Wei, H.X.; Zhang, W. Characterization of the generalized permeability jail in tight reservoirs by analyzing relative-permeability curves and numerical simulation. *Pet. Sci.* **2023**, *20*, 2939–2950. [CrossRef]
33. Gong, W.; You, L.; Xu, J.; Kang, Y.; Zhou, Y. Experimental study on the permeability jail range of tight gas reservoirs through the gas–water relative permeability curve. *Front. Phys.* **2022**, *10*, 923762. [CrossRef]
34. Assiri, W.; Miskimins, J.L. The Water Blockage Effect on Desiccated Tight Gas Reservoir. In Proceedings of the SPE International Symposium and Exhibition on Formation Damage Control, Lafayette, LA, USA, 26–28 February 2014; Society of Petroleum Engineers: Dallas, TX, USA, 2014. [CrossRef]
35. Nasriani, H.R.; Jamiolahmady, M. A Comparison of Clean-Up Efficiency of Multiple Fractured Horizontal Wells and Hydraulically Fractured Vertical Wells in Tight Gas Reservoirs. In Proceedings of the SPE Europec Featured at 80th EAGE Conference and Exhibition, Copenhagen, Denmark, 11–14 June 2018; Society of Petroleum Engineers: Dallas, TX, USA, 2018. [CrossRef]
36. Zhang, B.; Yang, D.; He, X. A unified model including non-Darcy flow and viscoelastic mechanisms in tight rocks. *Geophysics* **2022**, *87*, MR189–MR199. [CrossRef]
37. Balhoff, M.T.; Wheeler, M.F. A predictive pore-scale model for non-Darcy flow in porous media. *SPE J.* **2009**, *14*, 579–587. [CrossRef]
38. Vardian, M.; Nasriani, H.R.; Faghihi, R.; Vardian, A.; Jowkar, S. Porosity and permeability prediction from well logs using an adaptive neuro-fuzzy inference system in a naturally fractured gas-condensate reservoir. *Energy Sources Part A Recovery Util. Environ. Eff.* **2016**, *38*, 435–441. [CrossRef]
39. Abbasi, J.; Zhao, J.; Ahmed, S.; Jiao, L.; Andersen, P.Ø.; Cai, J. Prediction of permeability of tight sandstones from mercury injection capillary pressure tests assisted by a machine-learning approach. *Capillarity* **2022**, *5*, 91–104. [CrossRef]

40. Kathel, P.; Mohanty, K.K. Wettability alteration in a tight oil reservoir. *Energy Fuels* **2013**, *27*, 6460–6468. [[CrossRef](#)]
41. Brooks, R.H.; Corey, A.T. *Hydraulic Properties of Porous Media*; Colorado State University: Fort Collins, CO, USA, 1964.
42. Brooks, R.H.; Corey, A.T. Properties of porous media affecting fluid flow. *J. Irrig. Drain. Div.* **1966**, *92*, 61–90.
43. Dai, J.; Ni, Y.; Wu, X. Tight gas in China and its significance in exploration and exploitation. *Pet. Explor. Dev.* **2012**, *39*, 277–284. [[CrossRef](#)]
44. Gao, H.; Li, H.A. Pore structure characterization, permeability evaluation and enhanced gas recovery techniques of tight gas sandstones. *J. Nat. Gas Sci. Eng.* **2016**, *28*, 536–547. [[CrossRef](#)]
45. Freeman, C.M.; Moridis, G.J.; Ilk, D.; Blasingame, T.A. A numerical study of performance for tight gas and shale gas reservoir systems. *J. Pet. Sci. Eng.* **2013**, *108*, 22–39. [[CrossRef](#)]
46. Moridis, G.J.; Blasingame, T.A.; Freeman, C.M. Analysis of mechanisms of flow in fractured tight-gas and shale-gas reservoirs. In *SPE Latin American and Caribbean Petroleum Engineering Conference Proceedings*; Society of Petroleum Engineers (SPE): Dallas, TX, USA, 2010; pp. 1310–1331. [[CrossRef](#)]
47. Aguilera, R. Flow units: From conventional to tight-gas to shale-gas to tight-oil to shale-oil reservoirs. *SPE Reserv. Eval. Eng.* **2014**, *17*, 190–208. [[CrossRef](#)]
48. He, S.; Fang, F.; Song, K.; Li, X.; Zhang, J.; Cao, J.; Wang, Y.; Huang, X.; Bian, C. Research progress on the method of determining gas–water relative permeability curve in unconventional reservoirs. *J. Pet. Explor. Prod. Technol.* **2025**, *15*, 36. [[CrossRef](#)]
49. Sharifigaliuk, H.; Mahmood, S.M.; Zoveidavianpoor, M.; Zivar, D.; Afolabi, F.A. Experimental and Modeling Study of Water Imbibition and Flowback in Shale: Prediction of Relative Permeability and Capillary Pressure Curves. *Energy Fuels* **2023**, *37*, 11928–11941. [[CrossRef](#)]
50. Shen, W.; Ma, T.; Zuo, L.; Yang, X.; Cai, J. Advances and Prospects of Supercritical CO₂ for Shale Gas Extraction and Geological Sequestration in Gas Shale Reservoirs. *Energy Fuels* **2024**, *38*, 789–805.
51. Tian, J.; Chen, Q.; Qin, C.; Kang, Y.; Jia, N.; Xi, Z. Pore-scale systematic study on the disconnection of bulk gas phase during water imbibition using visualized micromodels. *Phys. Fluids* **2022**, *34*, 062015. [[CrossRef](#)]
52. Nasriani, H.R.; Moradidowlatabad, M.; Borazjani, A.A.; Nasriani, M. On the Revaporization of Retrograde Condensate by Gas Injection. In *Proceedings of the 79th EAGE Conference and Exhibition 2017, Paris, France, 12–15 June 2017*. [[CrossRef](#)]
53. Modebelu, E.C.; Nasriani, H.R.; Francis, J. Integrated Evaluation of the Clean-Up Performance of Unconventional Gas Plays; Investigating the Impact of Desiccation. In *Proceedings of the 83rd EAGE Annual Conference & Exhibition, Madrid, Spain, 6–9 June 2022*; European Association of Geoscientists & Engineers: Houten, The Netherlands, 2022; pp. 1–5. [[CrossRef](#)]
54. Nasriani, H.R.; Kalantari Asl, A. Two-phase flow choke performance in high rate gas condensate wells. In *Proceedings of the SPE Asia Pacific Oil and Gas Conference and Exhibition 2011, Jakarta, Indonesia, 20–22 September 2011*; Society of Petroleum Engineers: Dallas, TX, USA, 2011. [[CrossRef](#)]
55. Nasriani, H.R.; Kalantari Asl, A. Choke Performance in High-rate Gas Condensate Wells Under Subcritical Flow Condition. *Energy Sources Part A Recovery Util. Environ. Eff.* **2014**, *37*, 192–199. [[CrossRef](#)]
56. Gholami, S.; Rostaminikoo, E.; Khajenoori, L.; Nasriani, H.R. Density determination of CO₂-Rich fluids within CCUS processes. *Meas. Sens.* **2025**, *38*, 101739. [[CrossRef](#)]
57. Ghiri, M.N.; Nasriani, H.R.; Sinaei, M.; Najibi, S.H.; Nasriani, E.; Parchami, H. Gas Injection for Enhancement of Condensate Recovery in a Gas Condensate Reservoir. *Energy Sources Part A Recovery Util. Environ. Eff.* **2015**, *37*, 799–806. [[CrossRef](#)]
58. Nasriani, H.R.; Khan, K.; Graham, T.; Ndlovu, S.; Nasriani, M.; Mai, J.; Rafiee, M.R. An Investigation into Sub-Critical Choke Flow Performance in High Rate Gas Condensate Wells. *Energies* **2019**, *12*, 3992. [[CrossRef](#)]
59. Nasriani, H.R.; Jamiolahmady, M.; Alajmi, E. An Integrated Study of Cleanup Efficiency of Short Hydraulic Fractured Vertical Wells Using Response Surface Methodology. In *Proceedings of the 76th EAGE Conference and Exhibition 2014, Amsterdam, The Netherlands, 16–19 June 2014*. [[CrossRef](#)]
60. Medaiyese, F.J.; Nasriani, H.R.; Khan, K.; Khajenoori, L. Sustainable Hydrogen Production from Plastic Waste: Optimizing Pyrolysis for a Circular Economy. *Hydrogen* **2025**, *6*, 15. [[CrossRef](#)]
61. Nasriani, H.R.; Jamiolahmady, M.; Alajmi, E.; Ghahri, P. A Study of Hydraulic Fracturing Clean-up Efficiency in Unconventional Gas Reservoirs Using Statistical Approaches. In *Proceedings of the ECMOR XIV-14th European Conference on the Mathematics of Oil Recovery, Catania, Italy, 8–11 September 2014*.
62. Nasriani, H.R.; Borazjani, A.A.; Iraj, B.; MoradiDowlatabad, M. Investigation into the effect of capillary number on productivity of a lean gas condensate reservoir. *J. Pet. Sci. Eng.* **2015**, *135*, 384–390. [[CrossRef](#)]
63. Lai, F.; Li, Z.; Wang, Y. Impact of water blocking in fractures on the performance of hydraulically fractured horizontal wells in tight gas reservoir. *J. Pet. Sci. Eng.* **2017**, *156*, 134–141. [[CrossRef](#)]
64. May, E.A.; Britt, L.K.; Nolte, K.G. The Effect of Yield Stress on Fracture Fluid Cleanup Nolte, SPE, Dowell. In *Proceedings of the SPE Annual Technical Conference and Exhibition, San Antonio, TX, USA, 5–8 October 1997*. [[CrossRef](#)]

65. Lolon, E.P.; McVay, D.A.; Schubarth, S.K. Effect of Fracture Conductivity on Effective Fracture Length. In Proceedings of the SPE Annual Technical Conference and Exhibition, Denver, CO, USA, 5–8 October 2003; Society of Petroleum Engineers: Dallas, TX, USA, 2003. [CrossRef]
66. Zhao, J.; Ren, L.; Jiang, T.; Hu, D.; Wu, L.; Wu, J.; Yin, C.; Li, Y.; Hu, Y.; Lin, R.; et al. Ten years of gas shale fracturing in China: Review and prospect. *Nat. Gas Ind. B* **2022**, *9*, 158–175.
67. He, T.; Li, Z.; Jiang, F.; Hu, G.; Lin, X.; Lu, Q.; Zhao, T.; Shi, J.; Yang, B.; Li, Y. Simulation Study of Natural Gas Charging and Gas–Water Occurrence Mechanisms in Ultra-High-Pressure and Low-Permeability Reservoirs. *Energies* **2025**, *18*, 1607. [CrossRef]
68. Li, Y.; Jiang, G.; Li, X.; Yang, L. Quantitative Investigation of Water Sensitivity and Water Locking Damages on a Low-Permeability Reservoir Using the Core Flooding Experiment and NMR Test. *ACS Omega* **2022**, *7*, 4444–4456. [CrossRef]
69. Ghanbari, E.; Dehghanpour, H. The fate of fracturing water: A field and simulation study. *Fuel* **2016**, *163*, 282–294. [CrossRef]
70. Li, C.; Peng, Y.; Dong, J.; Chen, L. Prediction of the dew point pressure for gas condensate using a modified Peng–Robinson equation of state and a four-coefficient molar distribution function. *J. Nat. Gas. Sci. Eng.* **2015**, *27*, 967–978. [CrossRef]
71. Jing, G.; Chen, Z.; Hu, X.; Hui, G. Influence of different shut-in periods after fracturing on productivity of MFHW in Duvernay shale gas formation with high montmorillonite content. *Fuel* **2022**, *314*, 122719. [CrossRef]
72. Zhao, H.; Li, Z.; Zhu, C.; Ru, Z. Reliability analysis models for hydraulic fracturing. *J. Pet. Sci. Eng.* **2018**, *162*, 150–157. [CrossRef]
73. Zolfaghari, A.; Dehghanpour, H.; Ghanbari, E.; Bearinger, D. Fracture characterization using flowback salt-concentration transient. *SPE J.* **2016**, *21*, 233–244. [CrossRef]
74. Guo, J.-J.; Di, K.-X.; Zhang, L.-H.; Zhao, Y.-L.; Tang, H.-Y.; Zhang, R.-H.; Tian, Y. Insights into in-situ imbibition behavior of fracturing fluid in propped shale fractures based on nuclear magnetic resonance: A case study from Longmaxi Formation shale, Sichuan Basin, China. *Pet. Sci.* **2024**, *21*, 410–429. [CrossRef]
75. Erimako, R.J.B.; Nasriani, H.R.; Asimakopoulou, E.; Graham, T.L.; Whitty, J. Numerical Investigation of Hydraulic Fractures in Multiple Horizontal Wells: Analysis of Zipper & Modified Zipper Fracking. In Proceedings of the 83rd EAGE Annual Conference & Exhibition, Madrid, Spain, 6–9 June 2022; European Association of Geoscientists & Engineers: Houten, The Netherlands, 2022; pp. 1–5. [CrossRef]
76. *Geoquest, ECLIPSE 100*, version 2015.1.0.0; Schlumberger: Houston, TX, USA, 2015.
77. Thomas, L.K.; Katz, D.L.; Tek, M.R. Threshold pressure phenomena in porous media. *Soc. Pet. Eng. J.* **1968**, *8*, 174–184.
78. *Schlumberger Petrel E&P Software Platform*, version 2014.1 (64-bit); Schlumberger: Houston, TX, USA, 2014.
79. Schlumberger MEPO Multiple Realization Optimizer; MEPO4.2.0; Build:2617; Date: 2013-Apr-25_15-59. 2013, 4.2.0. Available online: <https://www.software.slb.com/products/mepo> (accessed on 19 June 2016).

Disclaimer/Publisher’s Note: The statements, opinions and data contained in all publications are solely those of the individual author(s) and contributor(s) and not of MDPI and/or the editor(s). MDPI and/or the editor(s) disclaim responsibility for any injury to people or property resulting from any ideas, methods, instructions or products referred to in the content.